An Atomistic Simulation towards Elucidation of Operating Temperature Effect in CO_2 Swelling of Polysulfone Polymeric Membranes

S.S.M. Lock [1], K.K. Lau *[1], A.M. Shariff [1], Y.F. Yeong [1], M. A. Bustam [1], Norwahyu Jusoh [1], Faizan Ahmad [2]

[1] CO_2 Research Center (CO2RES), Department of Chemical Engineering, Universiti Teknologi PETRONAS, Seri Iskandar, Malaysia

[2] School of Science and Engineering, Teesside University, Middlesbrough, United Kingdom

Corresponding author: laukokkeong@utp.edu.my

Abstract

A complementary study, which involves computational and in-house collected experimental work, has been employed to elucidate the swelling effect within polysulfone membranes by CO_2 at varying operating temperatures. The simulation models have been constructed with accordance to collected experimental data. The experimental and simulated sorption isotherms of CO_2 are in fairly good agreement with one another. Subsequently, the constructed molecular structures of unswollen and swollen polysulfone membrane at varying operating temperature has been analyzed to study the effect of CO_2 in terms of physical characteristic, glass transition temperature, relaxation and free volume to determine whether the temperature or concentration parameters are more dominant in CO_2 swelling. In addition, radial distribution function (RDF) between CO_2 and varying groups within polysulfone has been evaluated to determine association reaction that invokes the dilation. RDF at various operating temperature has been employed to be incorporated within a series of thermodynamic equations in order to quantify the interaction of CO_2 with polysulfone that constitutes to swelling.

Keyword: Molecular simulation, CO_2 swelling, operating temperature

1. Introduction

Membrane process is a recently emerged alternative in gas separation applied in natural gas purification as compared to traditional techniques, e.g. absorption, adsorption and cryogenics [1] attributed to its many benefits, such as flexible operating conditions, effective energy utilization and operating cost, chemical free as well as occupancy of smaller footprint [2-5]. Glassy polymeric membranes dominate membrane separation technology in an industrial scale since they have huge reproducibility for large scale production and low fabrication cost as compared to inorganic membranes [6], while exhibiting high gas selectivities alongside good mechanical characteristics in comparison to rubbery membranes [7]. Nonetheless, the drawback of adopting polymeric membrane is the occurrence of swelling effect, which has been rationalized through interaction between highly condensable gas molecules often existing as impurities in natural gas, e.g. CO_2, H_2S, and H_2O [8-17], with functional group of the polymeric chain [18]. Sorption of the gas molecules contributes to ease of movement for chain molecules to slide among each other, which constitute to enlargement in free volume of membrane matrix, consequently known as polymer softening [19, 20]. Hence, it becomes prominent to illuminate the swelling phenomenon since it is highly probable to cause alteration in membrane morphology that constitute to unwanted product lost, which decreases productivity of typical CO_2 separation from natural gas processing application [21].

Insight towards CO_2 induced swelling plays an essential role in development of separation efficiency and the molecular design of existing and next-generation polymeric membranes with desirable transport properties. As such, molecular simulation has been suggested as a viable substitute to offer elucidation towards morphology and properties of membranes from the molecular level, frequently realized through a combination of molecular dynamics (MD) and Monte Carlo (MC) methodology [22-25] following advancement in simulation and computational tools [18]. Moreover, adaptation of molecular simulation tool also overcomes the obstruction, expenditure and time in fabrication and empirical investigation of membrane through employment of experimental scale apparatus since it is found to be easier and direct to tune operating conditions of the simulation [26]. Nonetheless, to date merely a limited number of molecular simulation works have been dedicated towards unraveling CO_2 swelling effect to provide microscopic insight at a molecular level.

The feasibility elucidation of substantial interaction between gas molecule and polymeric system, which occurs typically at higher gas concentration levels, has been pioneered in work by van der Vegt *et al.* (1998), whence they considered a modified model of conventional polyethylene (PE) [27]. Based on the above motivation, Heuchel *et al.* (2006) initiated an effort to simulate unswollen and swollen states of polysulfone (PSF) and poly (ether sulfone) (PES) through generation of models with incorporation and without sorbed carbon dioxide [28]. Consequently, Hölck *et al.* (2006) correlated the PSF molecular structures at the reference states of unswollen and swollen conditions to the common dual sorption model and site distribution model of Kirchheim, which enabled quantification of CO_2 swelling induced behaviour in glassy polymers [29]. In another work by Hölck *et al.* (2008), they conducted molecular modelling in PSF and polyimide 6FDA-TrMPD (P14) structures to study the dilation effects induced by CO_2 swelling effect in varying types of polymer [30]. Spyriouni *et al.* (2009) introduced a new computational scheme to investigate the sorption and swelling characteristic of glassy atactic polystyrene (PS) at elevated pressures but reported requirement of more expensive computational procedures and tool to accomplish the simulation work [31]. In a subsequent work by Zhang *et al.* (2010), they investigated CO_2 induced swelling in 6PDA-ODA (6FDA = 4, 4-(hexafluoroisopropylidene) diphthalic anhydride, ODA = 4, 4-oxydianiline) polymeric membrane to realize a quantitative characterization between the polymer structure and its interaction with CO_2 molecules, which ultimately affected it separation performance [18]. In a similar work by Velioğlu *et al.* (2012), they extended the study of CO_2 swelling phenomenon to varying fluorinated polyimide membranes (e.g. 6PDA-ODA, 6FPA-DPX and 6FDA-DAM; DPX = 2,5-dimethyl-p-phenylenediamine, DAM = 2,4,6-trimethyl-m-phenylenediamine) [32]. Neyertz & Brown (2014) simulated *meta*-linked and *para*-linked 6FDA-6FmDA polyimide membrane to examine the CO_2 sorption and swelling resistant of isomeric structures [33, 34].

Based on review of published literatures, it is found that albeit acknowledgement of CO_2 swelling within glassy polymeric structures at the atomistic scale, the molecular simulation works have all been confined to study at ambient operating temperature of typically 308.15 K (35 °C). In typical natural gas processing, the entering natural gas are in the range of 30°C to 55°C in order to suit the temperature for membrane separation [35, 36]. The limitation thereby confines the understanding of CO_2 swelling phenomena at the fundamental level over an extended range of operating temperature from ambient condition,

which is frequently encountered in membrane gas separation industry [37]. The vitality of effect of operating temperature upon CO_2 induced swelling in gas transport properties have been affirmed through experimental observation by Duthie *et al.* (2007), whereby they reported solubility, diffusivity and permeability of gases through a swollen polyimide membrane at 21, 35, 50 and 77 °C respectively [38].

Nonetheless, operating temperature impacts on the CO_2 swelling phenomenon has been scarcely elucidated through molecular simulation work to provide phenomenological insight towards the thermal dependency on membrane morphology and interaction between CO_2 and functional group of the polymeric chains from molecular level. The relaxation process attributed to gas induced swelling behaviour at different operating temperature is dependent upon (i) the solubility of gas in the polymeric matrix and (ii) operating temperature of the system. In general, under isothermal conditions, the swelling effect is expected to be more apparent with increment of penetrant concentration in the membrane matrix. The higher gas concentration is typically encountered at lower operating temperature since solubility of gas decreases with increment in temperature attributed to higher affinity to maintain at the gaseous phase. On the other hand, mobility of polymeric chains may increase with higher temperature, which further induces accelerated swelling process. Both variables are interrelated and therefore substantiate in depth elucidation towards the membrane morphology and physical properties during the temperature dependent CO_2 swelling phenomena. Nonetheless, CO_2 swelling phenomena has been reported to be a reversible process, whereby membrane morphology returns to its original state once CO_2 is desorbed from the polymeric matrix [39]. The constraint prompts the requirement of in-situ observation of membrane to study the CO_2 swelling, which is difficult and costly through elipsometry technique to measure the free volume changes associated to CO_2 exposure and almost infeasible for study of CO_2 interaction with polymeric chain at a molecular level [40]. Hence, the question of operating temperature dependent swelling within polymeric membrane remains open and one that remains unravelled to date. It is not clear whether the temperature or gas concentration parameter is more dominant in the temperature dependent CO_2 swelling phenomena.

In this paper, a molecular modelling assemble has been conducted to simulate unswollen and swollen polysulfone (PSF) polymeric membrane structures characterizing the effect of CO_2 swelling at distinct operating temperatures, which are 30, 35, 40, 45, 50 and

55 °C, since it is one of the most commonly employed membranes in industrial application [41-43]. The studied temperature range is selected since it is typical operating temperature for natural gas purification and much lower than the glass transition temperature of PSF, which remains the polymeric membrane at glassy-like condition [44] to perform separation based on sorption and diffusion of gas penetrants [45, 46]. Simulated models have been constructed based upon inputs from in-house collected experimental data, such as operating conditions, amount of gas sorbed within the polymeric membrane matrix and structure density. Validity of the constructed polymeric membrane structures has been verified through good compliance observed between published or in-house experimentally measured and computationally simulated properties, such as density and sorption isotherms. Subsequently, physical properties characterizing effect of operating temperature towards extend of relaxation and swelling of polymeric membranes (e.g. physical structure, depression of glass transition temperature and mean square displacement of polymeric chains) have been elucidated. In addition, free volume of the constructed PSF membranes have been quantified [47], to address elucidation of temperature dependent swelling in polymeric membranes that remains unanswered in preceding simulation works. Interaction between CO_2 gas penetrants and PSF polymeric chain has been investigated to understand the functional groups that are responsible at incipient point of swelling. Finally, a mathematical correlation that quantifies the interaction of CO_2 and functional group of polymer at varying operating temperature has been proposed to quantify the swelling process in present work.

2. Methodology

In an overall, the methodology is comprised of coupling between experimental and simulation procedure to form a basis for correlation of molecular modeling work to actual membrane separation performance in order to further elucidate the temperature induced swelling effect. In this context, the molecular models have been simulated in accordance to measurement from laboratory condition. Applicability of the constructed models is further evaluated through comparison between simulated and experimentally measured sorption isotherms at varying operating temperatures. Subsequently, physical properties and morphology of the validated unswollen and swollen polymeric structures at varying operating temperatures have been elucidated. Overview of the methodology employed in present work is provided in Figure S1 in the Supplementary Information. In addition, few assumptions have been made in this work, such that the motion of atoms is describable by the law of

Newton's [48]. Other than that, the interaction between atoms is determinable by using the empirical potential functions [49]. Well-defined periodic boundaries in the x, y and z directions have been adapted to permit considerable simplification to the modeling process through assumption of homogenous characteristics throughout the polymeric membrane matrix [50].

2.1 Experimental Section

This section describes the materials and fabrication methodology to prepare PSF membrane employed in present study and pressure decay methodology for measurement of gas penetrants solubility within the fabricated PSF membrane matrix.

2.1.1 Materials and Membrane Preparation

The polysulfone (PSF) dense film was prepared via solution casting method using N-Methyl-2-pyyrolidone (NMP) as solvent [51-53] with a composition of 25 wt% PSF. The PSF was manufactured and supplied in pellet form by Aldrich (MW ~35000 by light scattering) while NMP from Merck (analytical grade) was used as received.

Initially, the PSF pellets were placed in a vacuum oven overnight to remove excess moisture trapped within the solids. Then, the dehydrated pellets were weighted on a Sartorius weighing scale (precision 0.1 mg) to determine the required amount. On the other hand, NMP solvent was measured and filtered using a 1.0 μm PTFE membrane filter to eliminate any undesirable contaminants and debris. The PSF pellets were then dissolved and mixed within NMP solvent for 24 hrs until the dissolution process has been completed, which was confirmed via the observation of a homogenous PSF/ NMP solution through naked eyes. Prior to casting, the mixed solution was desonicated within an ultrasonication water bath, which is operated at 120 W and 40 kHz, for 4 hrs and subsequently for 24 hrs of free standing degassing at ambient condition. The sonication and degassing procedure was conducted to remove any microbubbles formed during the mixing process to form a homogenous PSF/ NMP solution. The casting solution was then poured into a levelled and clean Petri glass dish. Subsequently, an aluminium foil was enveloped on the surface area of the Petri dish to minimize its evaporation rate. Drying protocol comprising of solvent evaporation process under atmospheric operating condition, and then annealing in vacuum oven via temperature

increment from 40 to 180 °C every 2 hrs with temperature interval of 20 °C has been carried out to avoid the creation of defects attributed to rapid solvent evaporation. Finally, the dried PSF membrane film was peeled off from the Petri dish with care.

2.1.2 Characterization of Membrane Sample

This section describes the characterization analyses that have been incorporated in current work to elucidate morphology of the fabricated membrane in order ensure its applicability prior to measurement of gas solubility behavior.

2.1.2.1 Variable Pressure Field Emission Scanning Electron Microscope (VPFESEM)

Morphology of the membrane samples were examined by variable pressure field emission scanning electron microscope (VPFESEM, Zeiss Supra 55 VP). Cross section images of the resultant membranes were obtained by using FESEM with an accelerating voltage of 10 kV. Cross sections of the membranes were prepared by submerging the samples in liquid nitrogen for several minutes before fracturing the film in order to obtain a clear and better image of the samples. All the membrane samples were subsequently sputter coated with platinum using Quorum Q150R S coater prior to imaging. Membrane samples were observed using VPFESEM with magnification from 300-3000.

2.1.2.2 Fourier transform infrared (FTIR)

The infrared (IR) spectra of the membrane sample were recorded using Fourier transform infrared spectrometer (Perkin Elmer Spectrum One), with 50 scans in the wavelength range of 450 - 4000 cm^{-1} under the transmission mode. The FTIR spectra were obtained using KBr method.

2.1.3 Solubility Measurement (Pressure Decay Methodology)

The principle is based on a dual-chamber pressure decay setup, which has been demonstrated in detailed elsewhere [54], in which the approach utilizes the concept of measuring the amount of gas initially in contact with a polymer sample and the amount of gas

remaining in the gas phase after equilibration. The methodology involves measurement of the resulting decrease in pressure as gas is absorbed into the polymer sample, the temperature of the sample and gas, and volume of the system in which the experiment takes place. In this study, in order to capture the impact of operating temperature to swelling induced sorption within polymeric membrane, the entire system has been submerged in a constant temperature water bath, whereby the temperature is constantly monitored and regulated at the designated operating condition of 30, 35, 40, 45, 50 and 55 °C respectively.

Theoretically, the dual chamber sorption system utilizes a reservoir chamber of known volume filled with gas to a known pressure, P_1, whereby the amount of gas, n_1, presents in the cell can be calculated using Eq. (1).

$$n_1 = \frac{P_1 V_{C1}}{Z_1 RT} \tag{1}$$

In Eq. (1), V_{C1} describes the inner volume of the chamber, T represents temperature of the gas, Z_1 is compressibility factor of the real gas under the designated operating condition (P_1 and T), which can be directly obtained or interpolated from established thermodynamic gas table, while R characterizes the ideal gas constant. In this study, the pressure P_1 has been regulated to up to 50 bars at an incremental step of 5 bars interval, to acquire the sorption behaviour of CO_2 in PSF membrane. A maximum pressure of 50 bars is required to constitute sufficient driving force in order to induce the swelling effect in PSF membranes [29, 30]. On the other hand, a second chamber that holds the polymeric membrane under study is located adjacent to the reservoir chamber. By opening a valve that separates both the reservoir and membrane chambers, the gas is allowed to flow into the second chamber and thus into the polymer. At the equilibrium point, when the sample is saturated, the pressure, P_2, will be relatively constant, and the amount of gas remaining in the reservoir and membrane chambers, n_{1+2}, can be conveniently calculated through employment of Eq. (2).

$$n_{1+2} = \frac{P_2(V_{C1}+V_{C2}-V_p)}{Z_2 RT} \tag{2}$$

In this context, V_{C2} corresponds to inner volume of the membrane cell, V_p is volume of the polymeric sample whereas Z_2 represents the compressibility factor at P_2 and T. Finally, the amount of gas dissolved into the polymer, n_p, can be determined as the difference of the initial amount of gas before sorption and the amount of gas remaining after sorption, such as that depicted in Eq. (3).

$$n_p = n_1 - n_{1+2} \tag{3}$$

The concentration of gas molecule, x, sorbed within the polymer membrane at any operating temperature has been obtained through Eq. (4), where 22414 cm^3/ mol corresponds to a simple numerical conversion factor and V_p (cm^3) is volume of the polymer sample in the membrane chamber, which has been determined through the conventional fluid displacement method in current work.

$$x = n_p\left(\frac{22414}{V_p}\right) \tag{4}$$

2.2 Molecular Simulation Section

The molecular simulation methodology in present work is subdivided into four parts. The first is molecular simulation treatment to construct the reference sates of unswollen and swollen PSF polymeric membrane structure at different operating temperatures, the second is procedure for determination of sorption of CO_2 gas molecules through Monte Carlo algorithm, third is glass transition temperature in the polymeric membranes, and the finally is analytical tool to evaluate free volume and cavity size distribution within the membrane matrix. All the molecular simulation works has been conducted using Materials Studio 8.0 software developed by Biovia [55].

2.2.1 Atomistic Packing Models

Polysulfone (PSF), which is a commercial membrane commonly adapted for gas separation, has been simulated employing a series of molecular dynamics (MD) procedure in Materials Studio 8.0. The repeating unit of the PSF polymeric membrane is provided in Figure 1.

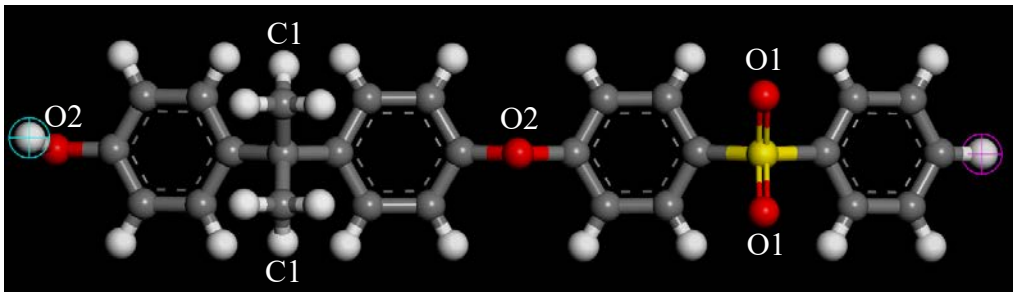

Figure 1 Single repeat unit for Polysulfone (PSF) polymeric chain, white: hydrogen, grey: carbon, yellow: sulphur, red: oxygen atom. Typical interaction sites with CO_2 under investigation (O1, C1 and O2) are shown.

The properties of the PSF polymeric membrane employed for molecular simulation study in present work has been summarized in Table 1 [56].

Table 1 Properties of PSF polymeric membrane for molecular simulation

Polymeric Membrane	PSF
Number of repeat unit	94
Number of polymeric chains	1
Experimental density (g/ cm^3)	1.24 [a]
Experimental glass transition temperature (°C)	186 [a]

[a] Experimental value by Ahn *et al.* (2008) [63].

To simulate the pure PSF membrane, PSF chain with head-to-tail orientation and isotactic tacticity has been employed consistently throughout the study. A PSF polymeric chain consisting of 94 repeat units is used as basis in all simulation works since it has been reported in previous work by Hölck *et al.* (2006) that this initial configuration can simulate bulk PSF polymeric membranes with relative great success at a fixed temperature of 308.15 K (35 °C) [28-30]. The same chain length has been employed but extended to different operating temperatures for ease of comparison and validation with previous published literatures [29]. A linear PSF polymeric chain has been simulated with the similar reasoning and basis as explained in our previous published literature [57].

The Condensed-phase Optimized Molecular Potentials for Atomistic Simulation Studies (COMPASS) force field has been employed constantly throughout the work. The COMPASS force field has been selected since it has been demonstrated in previous published works to be of sufficient reliability to simulate PSF membrane under the assumption of periodic boundary condition, which is in satisfactory accordance to actual experimental observation [57, 58]. The fundamental equation underlying the COMPASS force field is provided in equations (S1) – (S4) of Supplementary Information. The electrostatic

interactions have been characterized via the Ewald method (accuracy of 0.001 kcal/ mol), while the Lennard-Jones-6-12 function has been employed to describe the van der Waals interaction [59] with a cut-off-distance of ~18 Å (spline width of 1 Å and buffer width of 0.5 Å). The cut-off distance has been employed since it is lower than half of the anticipated cell specification, which has been suggested in previous published works to be adequate to prevent atoms interrelating with their own image, while minimizing computational cost [60-63]. All the electrostatic and Lennard Jones parameters have been extracted from Materials Studio simulation software for computational work. The computational study has been conducted from 3 initial configurations under all conditions, while the average has been reported to be statistically reliable.

2.2.1.1 Unswollen Polymeric Membrane Structure

The Forcite module of Materials Studio 8.0 has been employed to treat the initial polymeric chain through an energy minimization and geometry optimization protocol. In this context, the COMPASS force field has been employed together with the smart algorithm, which is a combination of the steepest descent; adjusted basis set Newton-Raphson (ABNR) and quasi-Newton algorithms in a cascading manner, in order to refine geometry of the initial polymeric chain. Later, the polymeric membrane chain has been folded into Amorphous Cell module adopting Construction task. The polymeric chain has been folded in the hypothetical cell by assuming PBC in all x, y and z directions at a value of 10% of the expected experimental density since initializing from a small density has been proposed to enhance the success rate of packing the polymeric chains at confined specification [64]. Moreover, it has been reported in published simulation works that the coupling effect of ring can be minimized via ramping from a low initial density [65-68]. In addition, small spacer molecules of 500 CO_2 have been packed in addition to the PSF polymeric chain during the initial phase of building amorphous cell, which can be removed in subsequent equilibration steps, to achieve the objective of minimizing the possibility of ring spearing and catenation during compacting process [69, 70]. Additionally, when constructing the polymeric membrane at low density through employment of the Amorphous Cell module, the function of checking for ring spearing and close contact has been enabled to prepare structures that are defects free prior to being subjected to a series of molecular treatment. During the molecular dynamics simulation process to gradually increase the structure to the targeted experimental density, the energy deviation tolerance has been set to a low value of 10000 kcal/mol since the phenomena of

ring coupling has been reported to induce excessive system energy [71, 72]. Rigorous checking for spearing and catenation of the ring has been conducted through employment of scripting available in Materials Studio [55]. All these procedures have been carried out with care to ensure that coupling effect of benzene ring has been avoided in all the final polymeric PSF membranes.

The basis adopted for packing and equilibration of polymeric membranes have been described in our previous works [57, 73] but devoted to construction of ultrathin Polysulfone at fixed operating parameters of 2 atm and 308.15 K. Firstly, all CO_2 from initial packing has been deleted prior to being subjected to the equilibration assemblies. In general, the initial constructed atomistic configuration without spacer molecules has been subsequently minimized and optimized adopting a series of protocols. Initially, in order to eradicate any unwanted atomistic arrangements, such as not feasible overlapping and close contact, a 10000 step energy minimization has been carried out. Subsequently, the polymeric membrane structures have been subjected to an annealing procedure through employment of the temperature cycle function embedded within Forcite module. In other words, temperature of the system has been increased from 353.15 K to 653.15 K with an interval of 20°C, and then from 653.15 K to 353.15 K, which corresponds to 15 heating ramps per cycle [74]. 100 ps isothermal-isobaric (NPT) has been performed at each designated temperature, which contributes to a total annealing simulation time of 3 ns. To maintain temperature and pressure (2 atm) of the molecular system at the designated operating conditions, the Nose thermostat with Q ratio of 0.01 and Berendsen barostat with decay constant of 0.1 ps have been employed continuously. After implementation of the thermal treatment, additional 25000 ps NPT molecular dynamics equilibration run has been conducted on the membrane cell to attain the most possible geometry and least energy structure. In a similar manner, the Nose thermostat and Berendsen barostat have been employed to coordinate the pressure at 2 atm while the temperature is fixed at the designated operating temperature (e.g. 303.15-328.15 K). Time step of 1 fs has been adapted to integrate the equation of motions via the velocity Verlet algorithm throughout the molecular dynamic steps. Subsequently, an additional 25000 ps of Canonical (NVT) ensemble has been conducted on the equilibrated polymeric structure at the studied operating temperature to eliminate any internal structural inhomogeneities and to ensure the structures have achieved metastable condition. The NPT-NVT protocols have been iterated in an alternate manner until alteration in the successive density values are within predefined tolerance. The unswollen polysulfone membrane structure is named PSFTC

throughout this study, with T being operating temperature of interest (e.g. PSF30C, PSF35C, PSF40C, PSF45C, PSF50C and PSF55C).

2.2.1.2 Swollen Polymeric Membrane Structure

Additional membrane structures have been simulated for the swollen polymer system with consideration of CO_2 at varying operating temperatures. To conform with the PSF polymeric chain of 94 repeat units, the respective loading taken from the sorption experiment in present work, n_{sim}, which has to be packed in addition to the simulation box, can be conveniently computed based on Eq. (5).

$$\mathrm{n_{sim}} = \mathrm{Abs}\left[\mathrm{x.\,v_{cell}}.\left(\frac{6.023\times10^{23}}{22414}\right)\right] \quad (5)$$

In Eq. (5), x is concentration of the sorbed CO_2 swelling agent within the polymeric membrane at varying operating temperature measured from our in-house experimental pressure decay setup, such as that explained in section 2.1.3, $\mathrm{v_{cell}}$ is volume of the simulation box, 6.023×10^{23} characterizes the Avogadros number and 22414 is the numerical conversion factor for gas at standard operating pressure and temperature. Similarly, 500 CO_2 gas molecules have been included with the PSF polymeric chain into the simulation box employing Construction task located within the Amorphous Cell module of Materials Studio 8.0. The number of CO_2 gas molecules at different operating temperature to be incorporated within the final packing model to induce the swelling effect at varying operating temperature is computed based on Eq. (5). Unlike the unswollen simulation model, deletion of CO_2 gas molecules have been conducted in a random manner until it reaches the number according to Eq. (5). The same molecular treatment and dynamic procedures, as highlighted in section 2.2.1.1, have been carried out on the swollen polymeric membrane structures. In order to simulate the effect of operating temperature to the CO_2 plasticization effect, the procedures are repeated at temperature of 303.15 K, 308.15 K, 313.15 K, 318.15 K, 323.15 K and 328.15 K (corresponding to 30, 35, 40, 45, 50 and 55 °C) respectively and at an operating pressure of 50 bars to comply with laboratory sorption condition. A subscript s has been employed to represent all the swollen structures, such as PSFTCs, in which T is the operating temperature. The swollen simulation structures for 30, 35, 40, 45, 50 and 55 °C have been referred to as PSF30Cs, PSF35Cs, PSF40Cs, PSF45Cs, PSF50Cs and PSF55Cs consistently later in this study. By removing the CO_2 penetrants molecules within the PSF membrane, simulation models are derived for the polymer matrix only, denoted by the index m, such as PSU30Csm,

PSF35Csm, PSF40Csm, PSF45Csm, PSF50Csm and PSF55Csm. These models would be tentatively employed to perform the grand canonical Monte Carlo ensemble (GCME) simulation, such as described in section 2.2.2, on the unswollen and swollen polymeric membrane at varying operating temperatures to recalculate the respective sorption isotherms, as well as to verify applicability of the simulation methodology via comparison with experimental densities.

2.2.2 Monte Carlo Sorption

In order to further validate accuracy of the simulated molecular structures, the solubility of CO_2 has been investigated employing the "fixed loading" task located in Sorption module of Materials Studio 8.0. As a whole, the simulation encompasses a series of grand canonical Monte Carlo ensemble (GCME), whence fugacity and temperature of the hypothetical cell are remained at a fixed value. General speaking, the framework is exposed to a reservoir with existence of infinite sorbate at the particular operating conditions assigned by end users. The Metropolis methodology [58, 75-77] has been adapted to include CO_2 into the preferred sorption sites, in which likelihood of inclusion has been calculated according to energy change between successive configurations, ΔE, such as that shown in equation S1 of the Supplementary Information [78]. Decisive factors that are included in the Metropolis algorithm for reception and denial of sorbate molecules include configurational moves (rotation and translation) as well as construction and destruction of sorbates [79]. Both van der Waals and Columbic electrostatic forces (non-bonded energy terms) are included in the sorption simulation. The Metropolis algorithm has been selected in current study since it has been demonstrated in previous published molecular simulation works to be an adequate characterization for system with relatively small sorbates as compared to pore size of the polymeric matrix and inherits low degree of torsion flexibility, which are highly applicable to CO_2 gas molecules [58, 80].

2.2.3 Glass Transition Temperature

In this study, the temperature cycle in Forcite Module of Materials Studio 8.0 has been employed to determine the T_g. Firstly, the final PSF membrane structures for unswollen and swollen reference states at varying operating temperatures have been entitled to an extra

10 ps Canonical (NVT) ensemble with a time step of 1 fs, which enabled 10 frames in a trajectory file format to be obtained for each membrane structure. In other words, an average T_g can be computed to enhance accuracy of the value when the series of thermodynamic treatment is repeated while computing a distinct T_g for each frame. In this context, numerous cycles of NPT run at different operating temperatures have been conducted on the membrane structures, while its density alteration at each independent temperature has been plotted to determine the crossover point from glassy to rubbery region, which defines the T_g. The independent frame in the PSF trajectory document has been heated from 300.15 K to 500.15 K via NPT dynamics at different temperature with an interval of 1 K. A NPT dynamic simulation run of 1 fs time step and total simulation time of 1000 ps has been implemented at each designated temperature and operating pressure (2 bars and 50 bars for unswollen and swollen PSF simulation model respectively). After the heating protocol, the membrane system is cooled from 500.15 K to 300.15 K with a temperature interval of 1 K employing the exact identical NPT molecular dynamics simulation, while determining density at each operating condition. The procedure is iterated throughout the frames in the PSF trajectory file and the average values are determined when approaching the end of the simulations.

2.2.4 Fractional Free Volume

Two independent states have been recognized in polymeric membranes, which encompass a solid phase made up by polymeric chains and an empty space region, which is frequently called the free volume [56]. It is vital to provide an understanding towards the void space within the polymeric membrane, since it forms the channel for passage of gas penetrants [81]. To enumerate the quantity of void region within the membrane matrix, the fractional free volume (FFV) is a useful variable with its definition provided in (6).

$$FFV = \frac{v_g - v_o}{v_g} \tag{6}$$

In equation (6), v_g is specific volume of the polymeric glass at a specific operating condition and v_o is occupied volume of the polymer chain.

The Connolly Surface function inherent in Materials Studio 8.0, with an input of medium grid resolution and 0.4 Å grid intervals, has been utilized to separate regions of occupied polymeric chains and free volume [82, 83]. The Connolly probe radius is altered to fit the FFV calculated via Bondi's methodology for the PSF30C membrane structure, with the

same value being subsequently employed for all unswollen and swollen structures at different operating temperatures. FFV (Bondi) parameter has been generally evaluated based on Bondi's group contribution methodology, such as that depicted in expression (7) [84].

$$v_o = 1.3 \sum_{k=1}^{n} (v_w)_k \quad (7)$$

In expression (7), n is total number of functional groups into which the repeat unit structure of a polymer is divided, while $(v_w)_k$ is van der Waals volume of the group, such as that proposed by Van Krevelen [85]. The specific volume of the PSF polymer films has been computed based on reciprocal of the simulated density from MD simulation, while v_o = 0.6903 cm^3/ g has been employed consistently for all conditions in current work for FFV (Bondi) computation.

3. Results and Discussion

This section discusses the results pertinent to CO_2 induced swelling within PSF polymeric membranes at different operating temperatures obtained from present study, which has been broadly subdivided into two major sections, such as those of experimental report and simulation analysis.

3.1 Experimental Work

To understand the fabricated membrane morphology, VPFESEM and ATR-FTIR have been conducted to analyze the fabricated membrane, with information related to characterization instrument found in section 2.1.2. From Figure 2, it is found that the PSF membrane is consisted of a dense single polymer layer that is homogenous and defects free in all directions.

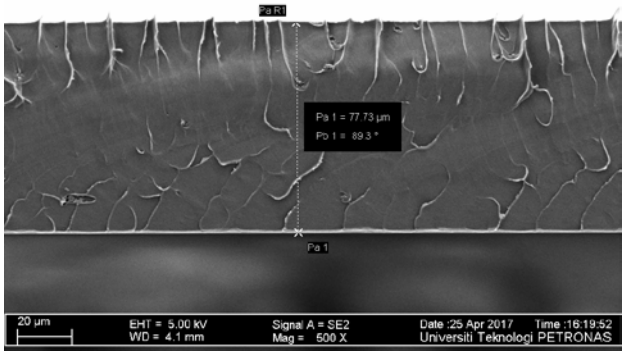

Figure 2 Cross sectional of PSF dense membrane

In addition, the functional groups obtained from ATR-FTIR, as demonstrated in Table 2, are consistent to the observed repeat unit of PSF (Figure 1). The good accordance demonstrates the validity of the synthesized PSF membrane and elimination of any impurities/ solvent that can potentially affect the membrane separation performance in later study.

Table 2 Characteristic of FTIR characterizing varying functional groups in fabricated PSF membrane

Functional group	Bands
Diaryl sulfone	1154, 1295, 1364
Diaryl ether linkage stretch	1250
Aromatic rings stretch	1485, 1587
Aliphatic C-H stretch	2857, 1387
Aliphatic C-H scissoring and bending	1410
Phenyl ring substitution band	693, 716, 738, 796, 837, 854
Aromatic C-H stretch	3037, 3067, 3094
Amide stretch	1685
Amines stretch	1081, 1109, 1295

To induce thermal dependence of CO_2 swelling in PSF membrane, the solubility of CO_2 penetrant within the polymer matrix has been measured through employment of the pressure decay methodology as outlined in section 2.1.3. Using the apparatus detailed earlier, solubility was determined, with CO_2 uptake by PSF measured as a function of penetrant across a range of temperature from 30 to 55 °C, such as that provided in Figure 3. Experimental data by Sada *et al.* (1988) that studied the effect of operating temperature to the solubility of CO_2 within PSF has also been provided in Figure 3 as reference [86]. In an overall, it is depicted that the collected sorption data of present study is not substantially different from the reported values by Sada *et al.* (1988), which demonstrates that the fabricated PSF polymeric membrane and experimental setup are of sufficient realibity to obtain defects free expeimental results. The sorption data of present work is consistently higher than that reported by Sada *et al.* (1988) at different operating temperatures, which can be deduced via the difference in source of Polysulfone to prepare the membrane samples.

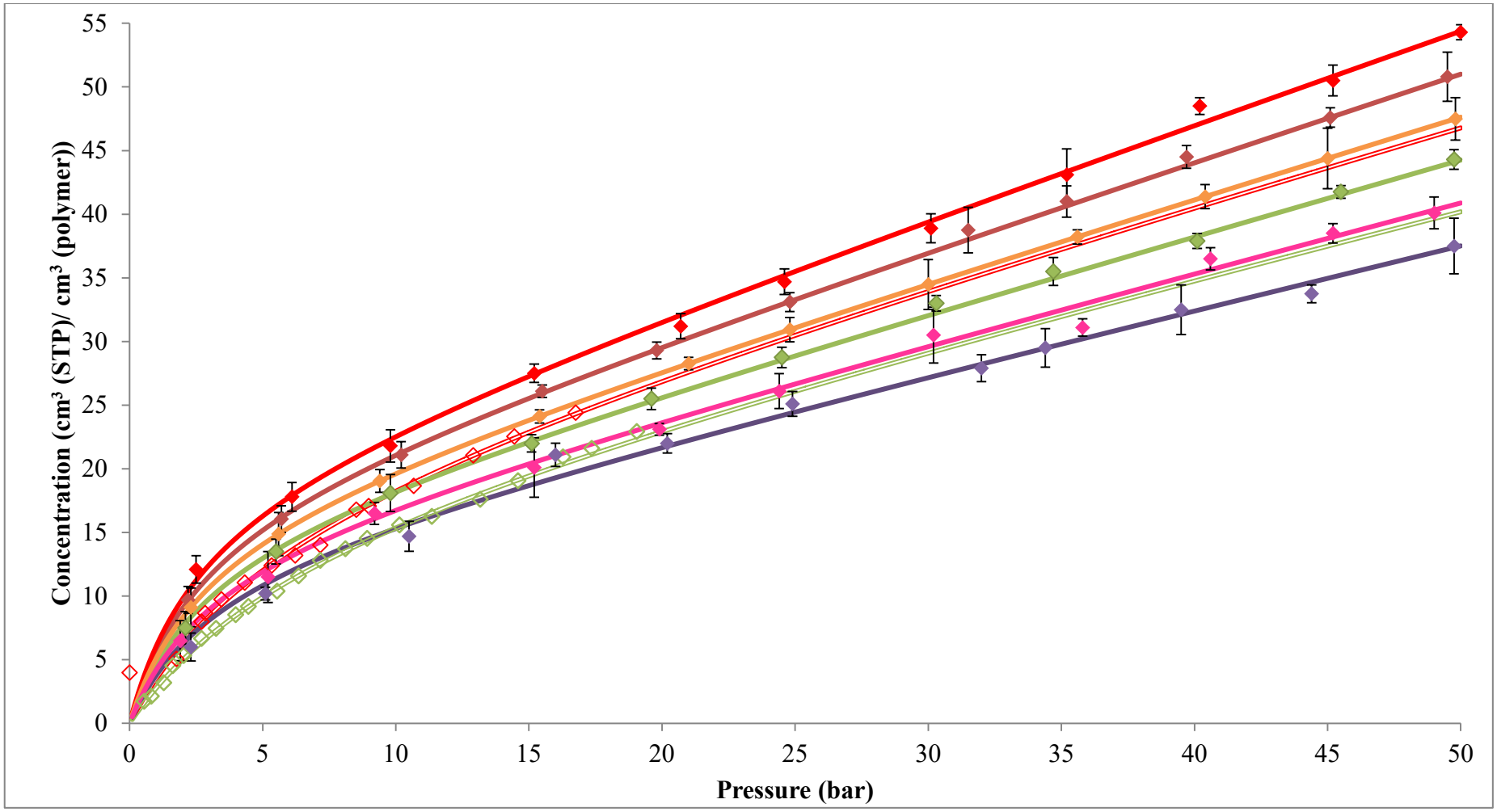

Figure 3 CO_2 sorption isotherm for polysulfone. Symbols represent experimental data while solid line depicts the dual model sorption model given by Eq. (8) with parameters as summarized in Table 3. Closed symbols characterize data from present study, whereas opened symbols are reported values by Sada *et al.* (1988) (Red – 30 °C; Maroon – 35 °C; Orange – 40 °C; Green – 45 °C; Pink – 50 °C; Purple – 55 °C)

It is depicted from Figure 3 that concentration of CO_2 within the polymeric matrix increases with increment in pressure regardless of the operating temperature, which has been rationalized through higher driving force that promotes the sorption of solvent. Being consistent to majority of glassy polymeric membranes, the PSF membrane is measured to inherit decreasing solubility with increment in operating temperature [86-90]. The observation has been attributed to the nature of gas molecules to sustain in its gas state rather than being sorbed within the polymeric matrix at higher operating temperature. In addition, the simulated gas sorption for CO_2 has been fitted with good accordance to the well-known dual mode sorption model correlation, such as that shown in Eq. (9).

$$C_i = C_{Di} + C_{Hi} = k_{Di}p + \frac{C'_{Hi}b_i p}{1+b_i p} \quad (9)$$

The dual mode sorption model suggests that the total concentration of gas i in a polymer matrix is composed of two idealized molecular scale environment, in which C_i is the total concentration of gas in the polymer; C_{Di} is equilibrium population existing in the polymer matrix under the dissolved mode and is governed by Henry's Law equation, while C_{Hi} is the non-equilibrium population existing in excess within the hole-filling environment governed by Langmuir parameters [91, 92]. Moreover, k_{Di} is the Henry's law coefficient that characterizes dissolution of a pure gas, i, in the polymer, b_i and C'_{Hi} is the Langmuir hole affinity parameter and the capacity parameter respectively, while p_i is pressure of the gas system [92-94]. The fitted dual mode sorption parameters are provided in Table 3, which has been summarized alongside the reported values by Sada *et al.* (1988) [86]. In has been demonstrated from Table 3 that the parameters are in satisfactory agreement with one another, attributed to the small distinction of the solubility characteristics as a whole. The good compliance with previous published literatures and fit to the commonly employed dual mode sorption model demonstrates that the measured solubility data are of adequate dependability as input for molecular simulation and model validation, which will be elaborated and discussed in subsequent sections through employment of Eq. (5).

Table 3 Dual-mode sorption parameters for carbon dioxide in polysulfone film as a function of operating temperature

Temperature (°C)	k_{Di} (cm^3(STP) $cm^{3-1}bar^1$)	b_i (bar^{-1})	C'_{Hi} (cm^3 (STP) cm^{3-1})
30	0.7202 (0.646) [b]	0.3810 (0.195) [b]	19.33 (20.5) [b]
35	0.6748 (0.595) [b]	0.3678 (0.178) [b]	18.20 (19.4) [b]
40	0.6294 (0.547) [b]	0.3546 (0.168) [b]	17.07 (18.3)
45	0.5840 (0.508) [b]	0.3415 (0.155) [b]	15.93 (17.1) [b]
50	0.5386	0.3283	14.81
55	0.4932	0.3152	13.67

[b] The number in bracket is the experimental value by Sada *et al.* (1988)

3.2 Molecular Models

This section discusses the results that have been obtained through molecular simulation of swollen and unswollen PSF structures at varying operating temperature. It has been subdivided into several sections, such as 1) amorphous cell structure 2) glass transition temperature and relaxation 3) free volume 4) radial distribution function and 5) interactions of CO_2-polymer system. All the physical properties have been quantified with respect to unswollen membrane at its respective operating temperature to compare the effect of mere temperature and simultaneous operating temperature and CO_2 gas concentration to the relaxation of polymeric chains.

3.2.1 Amorphous Cell Structure

As described in section 2.2.1.1, molecular dynamics simulation has been executed for unswollen PSF polymeric films by keeping the operating parameters at the designated values while the other structure configurations are constantly updated in quest of determining the

most probable polymeric membrane with optimized packing and molecular arrangement. On the other hand, the swollen structures have been constructed through incorporation of CO_2 loadings, which has been computed based on in-house measured CO_2 solubility in PSF membranes, such as that in discussed in section 3.1, and the molecular simulation procedure outlined in section 2.2.1.2. The number of CO_2 molecules employed in present study has been summarized in Table 4 [56, 74, 95, 96], whereby the computed value decreases when temperature increases, which has been rationalized through the reduction in affinity for dissolution within membrane matrix as elaborated in previous section.

Table 4 Density and specification of simulated and experimentally measured unswollen polysulfone membrane (PSFTC) and swollen polysulfone membrane with inclusion of the targeted CO_2 gas molecules (PSFTCs), as well as with after removal of CO_2 (PSFTCsm)

Operating temperature (°C)	Unswollen model				Swollen model				Dilation (%)
	Box length (Å)	ρ_{PSFTC} (g/cm^3)[c]	ρ (g/cm^3)[d]	Error (%)	n_{sim}	Box length (Å)	ρ_{PSFTCS} (g/cm^3)[e]	$\rho_{PSFTCSm}$ (g/cm^3)[f]	
30	38.192	1.2373	1.2341	0.2657	83	39.049	1.262	1.1602	6.6454
35	38.206	1.2360	1.2327 (1.240)[h]	0.2653	81	39.034	1.261	1.1614	6.4233
40	38.220	1.2347	1.2314	0.2651	76	39.012	1.257	1.1635	6.1195
45	38.233	1.2333	1.2301	0.2648	71	38.990	1.253	1.1654	5.8263
50	38.247	1.2320	1.2287	0.2645	65	38.923	1.252	1.1715	5.1643
55	38.261	1.2307	1.2274	0.2642	60	38.900	1.248	1.1735	4.8743

[c] Density of simulated unswollen PSF membrane at varying operating temperature
[d] Density of unswollen PSF membrane predicted through Tait's empirical models [95] obtained from Zoller's experimental data [74, 96]
[e] Density of swollen PSF membrane packing with inclusion of targeted number of CO_2 molecules
[f] Density of swollen PSF membrane matrix after removal of CO_2 molecules
[h] Experimental value by Ahn *et al.* (2008) [56]

Examples of the unswollen and swollen PSF amorphous simulation cell are provided in Figure **4**.

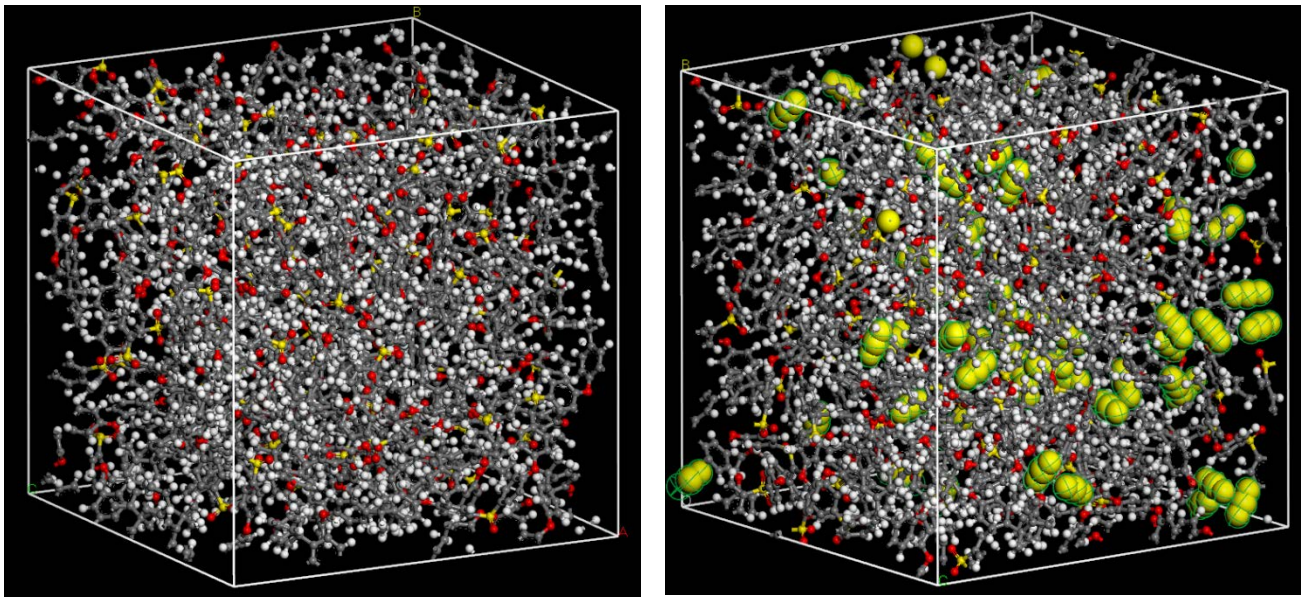

Unswollen PSF

Swollen PSF at varying operating temperatures with different number of CO_2

Figure 4 Molecular structure of unswollen and swollen PSF membrane structure at varying operating temperatures through input of different number of CO_2 gas molecules in accordance to experimental data obtained through molecular simulation in Materials Studio 8.0 software

As can be seen from Figure **4**, for the swollen PSF structures, the CO_2 gas molecules are randomly dispersed throughout void space within the PSF polymeric matrix, with the configuration corresponding to the optimized and most probable intermolecular interactions between the penetrants and polymeric chains.

Since the system has been initialized from lower density without setting any constrictions throughout the molecular dynamics treatment, the evolution of structure (e.g. energy and density) to a stable value provides intuitive reasoning that the polymeric membrane has converged towards the most plausible configuration. Hence, by analyzing physical property of the finalized molecular structure to theoretically attained value, which has been measured through published experimental simulation work, accuracy of the molecular simulation methodology can be validated. Example of density and energy

alternation during the course of one cycle of NPT molecular treatment for unswollen PSF membrane film has been provided in Figure 5.

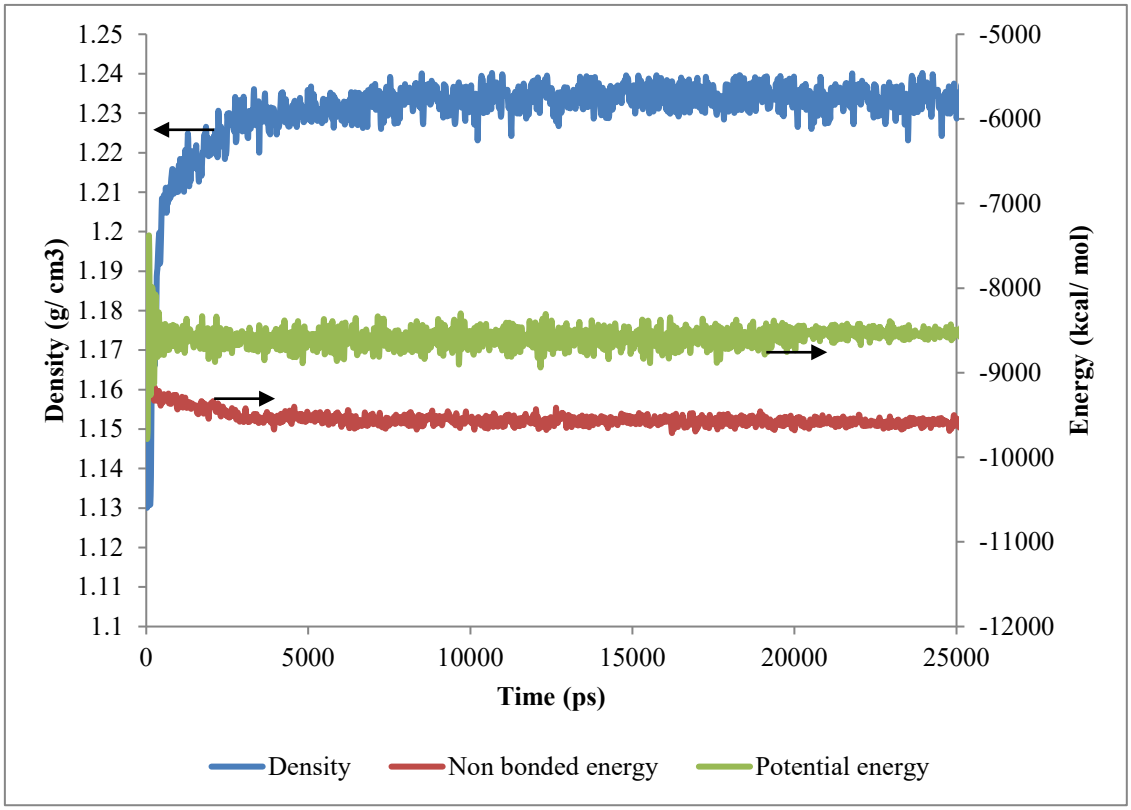

Figure 5 Evolution change during molecular dynamics simulation for density, non-bonded and potential energy for unswollen PSF membrane structure (Example of a one cycle 25000 ps NPT molecular treatment has been provided to guide the reader)

From Figure 5, it is found that the total potential energy and non-bonded contribution are found to experience decrement since the most plausible molecular structure is the one with the least energy configuration. When the molecular system surpasses approximately 5000 ps time steps, the energy parameters are reduced to values of approximately -8500 kJ/ mol and 9700 kJ/ mol (versus -8700 kJ/ mol and -9000 kJ/ mol in Golzar *et al.* (2014) study for molecular simulation of bulk PSF membranes in their study) [58], whence the amount of fluctuations is minimized when the NPT run proceeds, suggesting that the systems have reached thermodynamic equilibrium. In addition, it is also depicted that the density curves are nearly fixed within the range of 1.235 g/ cm^3 after 5000 ps of molecular treatment.

In order to validate accuracy of the developed PSF structures, densities of the simulated membrane, (e.g. PSFTC), with T being the studied operating temperature, have

been compared to experimentally measured values. To quantify accuracy of the simulation methodology, the percentage errors between the simulated and measured density, $\in$, has been provided for PSF membranes at varying operating temperatures, whereby the definition has been provided in (10).

$$\in = \frac{\rho_{PSFTC} - \rho}{\rho} \times 100\% \tag{10}$$

In (10), ρ_{PSFTC} describes density of the simulated unswollen membranes at varying operating temperature T, while ρ characterizes the computed density from Tait's empirical models [95] obtained via Zoller's experimental data [74, 96]. The equation has been provided in (11), which has been demonstrated to be particularly successful to provide a convenient mathematical characterization of pressure-volume-temperature (PVT) behavior for PSF membranes over a wide range of operating conditions. In (11), T characterizes the temperature in °C while P is the pressure in kg/ cm^2. In addition, previously reported experimental density of bulk PSF with a value of 1.24 g/cm^3 by Ahn *et al.* (2008) at 35 °C has also been provided as reference [56].

$$\rho = \frac{1}{(0.8051 + 1.756 \times 10^{-4} T)\left\{1 - 0.0894 ln\left[1 + \frac{P}{4408 exp\left(-1.543 \times 10^{-3} T\right)}\right]\right\}} \tag{11}$$

The good compliance between simulated and experimentally observed condition as demonstrated in Table 4 supports the claim that the unswollen PSF polymeric structure has been constructed via high accuracy simulation procedure since the system has been ramped from a low density configuration without confining any constraints and boundaries throughout the molecular dynamics process. Percentage error between simulated and experimentally observed PSF density from Tait-Zoller's expression and experimentally measured density by Ahn *et al.* (2008) can be rationalized through the assumption in molecular simulation, whence cut off distance has been applied throughout the simulation cell that deemed long range molecular interaction to be negligible. Tentatively, it is found that the molecular simulation tool is of sufficient capability to capture the trend characterizing effect of operating temperature to the density of molecular structure, such that the density decreases with increment in temperature. The observation can be rationalized through expansion of the simulation cell when operating temperature is raised attributed to higher activation energy for relaxation [96, 97].

The physical properties of the final optimized and equilibrated structures for swollen PSF30Cs, PSF35Cs, PSF40Cs, PSF45Cs, PSF50Cs and PSF55Cs are also provided in Table **4**. It has been depicted in Table **4** that the packing density of molecular structure increases with increment in CO_2 loadings, which is in the order of PSF55Cs < PSF50Cs < PSF45Cs < PSF40Cs < PSF35Cs < PSF30Cs. The observation tallies with characteristic of single packing models of PSF, as reported by Heuchel *et al.* (2006) [28], whereby PSF molecular structure with higher CO_2 loading exhibits greater packing density attributed to the presence of CO_2 that increases weight of the entire molecular system. Furthermore, density of the membrane matrix has been calculated after removal of the randomly distributed CO_2, whence the chronological sequence is in the order of PSF30Csm < PSF35Csm < PSF40Csm < PSF45Csm < PSF50Csm < PSF55Csm. Density of the membrane matrix experiences a decrement when CO_2 loadings are further increased in polysulfone located within lower operating temperature. The reduction in density of membrane matrix has been acclaimed through enhanced interaction between increased number of CO_2 gas molecule and polymeric matrix, which contributes to augmented swelling and relaxation in polymeric membrane structure [98]. The extend of relaxation has been quantified through the percentage dilation, ε, whence it has been computed based upon equation (13).

$$\varepsilon = \left(\frac{\rho_{PSFTC}}{\rho_{PSFTCSm}} - 1\right) \times 100\% \tag{13}$$

It is found that the percentage dilation rises with number of CO_2, which has been computed and tabulated in Table **4** as well, in which it is the lowest at operating temperature of 55 °C and increases with decrement in temperature. It is found that the dilation is especially apparent beneath operating temperature of 45 °C, whereby the percentage dilations achieves approximately 6 %. The observation can be rationalized through the proposal that a critical concentration of CO_2 is present in order to induce augmented swelling in polymeric membranes [98]. At higher operating temperature, majority of the CO_2 remains in it gaseous state, whereby the threshold to invoke the enhanced swelling effect has not been reached yet. This claim would be studied in an in-depth level through section 3.2.5 to provide insights from an atomistic level towards the interaction between CO_2 and varying functional groups of PSF. The smaller percentage dilation between the swollen and unswollen membrane state at higher operating temperature suggests that the concentration parameter is a more dominant parameter that governs the swelling phenomena in comparison to operating temperature, owing to the fact that it exhibits a lower density at the unswollen state but is expanded to the least extent in swollen condition with inclusion of less concentration of CO_2. The proposal

will be further affirmed through study of molecular structure and membrane morphology at subsequent sections.

3.2.2 Monte Carlo Sorption

It has been well addressed in previous sections that the sorption of CO_2 gas molecules at elevated pressure of 50 bars is accompanied by swollen and dilation of membrane structure as compared to its pristine unswollen counterpart. Therefore, in this section, the sorption capacity of the unswollen (PSFTC) and swollen polysulfone membranes at varying operating temperatures with removal of all gas penetrants (e.g. PSFTCsm) have been conducted according to the GCMC algorithm in order to study the effect of CO_2 induced swelling towards the transport property, as well as to further verify accuracy of the simulated structures through comparison with in-house measured experimental results. Similar approach has been adapted in previous works by Heuchel *et al.* (2006) [28], Hölck *et al.* (2006) [29], Zhang *et al.* (2010) [18] and Velioğlu *et al.* (2012) [32] to achieve the objective of understanding the influence of CO_2 swelling to sorption behaviour of varying glassy polymers, while validating applicability of the unswollen and swollen polymeric membrane as reference points. Example of the sorption behaviour based upon the PSFTC and PSFTCsm membrane matrix structure at 30 °C is provided in Figure **6**, while the other operating temperatures have been provided in Figure S2 of supplementary information for reader's guidance.

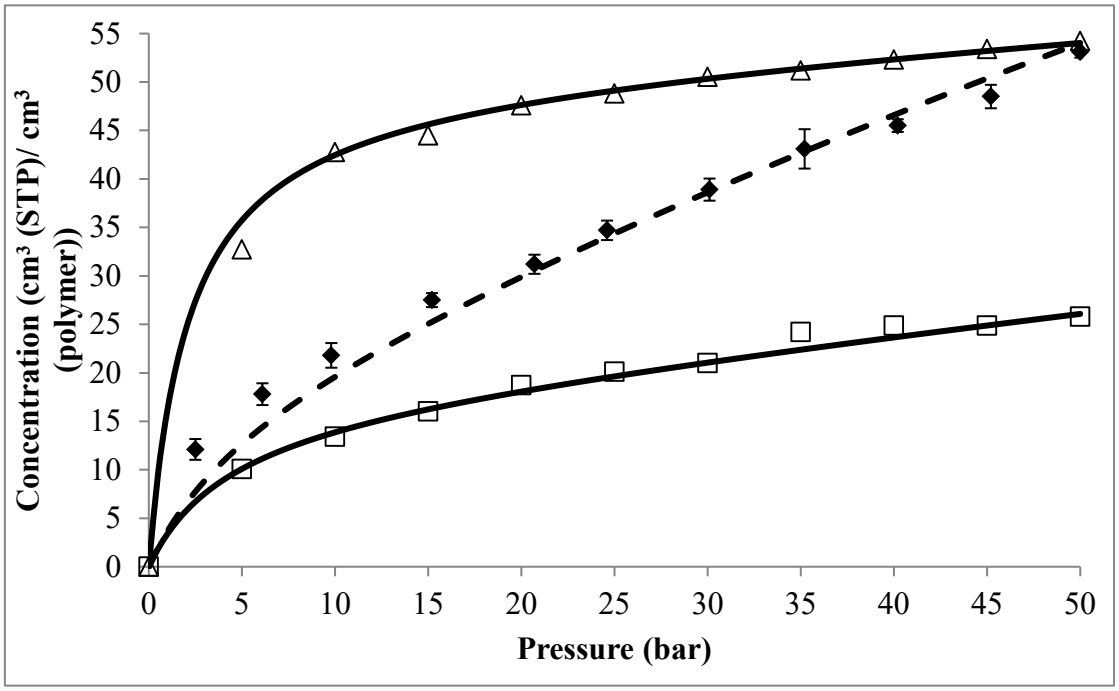

Figure 6 Sorption isotherm at 30 °C calculated for unswollen Polysulfone - PSF30C (□) and swollen Polysulfone - PSF30Csm (△) packing models; experimental data (◆); dual mode sorption model (—); linearly weighted average fit (- - -)

It is seen from Figure **6** that the unswollen model (PSF30C) only shows good compliance to the experimental data in the low pressure range (< 2 bars), while the opposite is demonstrated in the swollen model (PSF30Csm), whereby overestimation of prediction has been observed. Only the point at 50 bars, the swollen membrane depicts good accordance to experimental results since the structure is designed to accommodate actual experimental condition at the indicated pressure. The observation can be rationalized through dilation of the membrane structure when exposed to CO_2 gas penetrants from low to high pressure, whereby CO_2 interacts with functional group of the PSF polymeric chain. The interaction contributes to likelihood of lack of efficient packing in polymeric membrane with increment in operating pressure, which acts as site for absorption of gas molecules. On the other hand, the smaller number and size in cavities that are created in the denser PSF polymeric membrane structures at unswollen state, behave as potential barrier against the entrance of sorbents by means of causing molecular hindrance to allow smaller number of gas molecules that have surpassed the minimum energy requirement to pass through the impediments and finally being sorbed into the membranes. The claim in free volume morphological alterations from unswollen to swollen structures at varying operating temperature would be further discussed in section 3.2.4. Difference between the sorption isotherm of the unswollen and swollen state is most apparent at lowest operating temperature of 30 °C, whereby the effect levels off with increment in operating temperature. This observation supports the claim that gas concentration is a more prominent factor in determining swelling effect in polymeric membrane as compared to operating temperature since the deviation at lower temperature (lower activation energy and relaxation) and higher CO_2 concentration is more obvious.

In is found that mere slight deviation (< 4%) is observed between the experimentally measured and simulated sorption at 50 bars based upon PSFTCsm, whereby the simulated extend of sorption is found to be consistently larger than the experimental measurement, such as that summarized in Table **5**.

Table 5 Validation through good compliance observed between simulated and experimental obtained sorption data for unswollen and swollen PSF membranes at varying operating temperature

Simulated structure	Simulated concentration (cm^3 (STP)/ cm^3 (polymer))	Experimental measured concentration (cm^3 (STP)/ cm^3 (polymer))	Error (%)
PSF30Csm	54.2	53.1	2.07
PSF35Csm	52.2	50.8	2.76
PSF40Csm	49.2	47.5	3.58
PSF45Csm	46.0	44.3	3.84
PSF50Csm	41.5	40.3	2.98
PSF55Csm	38.4	37.5	2.40

Similar observation has been reported in Zhang *et al.* (2010) [18] simulation work as a consequence of several plausible reasoning. The first constraint is related to the time scale of MD simulation, whence it is merely restricted to relatively short simulation times (roughly in the regime of several pento to nanoseconds) to resolve atomic vibrations. On the other hand, relaxation rate has a strong effect on the resulting properties attributed to the time-dependent response of amorphous polymers, which needs to be accounted for when comparing MD simulations and experiments [99]. Consequently, relaxation rates are many orders of magnitude faster than those normally used in experiments, which constitute to deviation between simulation and actual laboratory observation. Secondly, the rates of reaching steady state between molecular simulation and experimental are considerably distinct. In the simulation condition, CO_2 gas molecules are directly inserted into the favourable sites of membrane matrix, while in actual membrane transport mechanism, it is based upon the solution diffusion theory, whereby gas components dissolve within a particular membrane material at the high pressure side, permeate across the membrane through a driving force and finally evaporate from the low pressure end [100]. All these contributed to possible deviations between simulated and experimentally observed conditions but the errors are within predefined tolerance to be employed for elucidation of operating temperature effect in CO_2 swelling of PSF membranes. In addition, trend with respect to effect of operating

temperature to the induced sorption effect, such as augmented solubility in swollen PSF structures as compared to its respective unswollen state and reduced solubility in swelled PSF membrane with increment in operating temperature, has been captured effectively by the simulation models.

For intermediate pressures, the assumption of a linear change in density with pressure has been adapted to describe the transition from PSFTC to PSFTCsm, in which the evolution can be quantified through a linearly weighted average correlation between both the isotherms [18, 32], such as that depicted in Eq. (14).

$$C(p) = \left(1 - \frac{p}{p_{PSFTCsm}}\right) C_{PSFTC}(p) + \frac{p}{p_{PSFTCsm}} C_{PSFTCsm}(p) \quad (14)$$

In this context, $C(p)$ is concentration of CO_2 gas penetrants within the polymeric matrix at that study (50 bars), $C_{PSFTC}(p)$ and $C_{PSFTCsm}(p)$ are the calculated concentration solubility data points at unswollen and swollen conditions at each operating temperature T respectively. All the sorption behavior at different operating temperatures, regardless of being the unswollen or swollen membrane structures at 50 bars, can be conveniently described through employment of the dual mode sorption model, as depicted in Eq. (9). It has been proposed that the dual mode parameters are a function of temperature through the Van't Hoff expression [38, 98, 101, 102]. By incorporating the temperature dependent dual mode parameters into expression (14), the correlation as a function of temperature is presented in equation (15).

$$C(p) = \left(1 - \frac{p}{p_{PSFTCsm}}\right)\left[k_{Di,0(u)}\exp\left(\frac{\Delta H_{D(u)}}{RT}\right)p + \frac{C'_{Hi,0(u)}\exp\left(\frac{\Delta H_{C(u)}}{RT}\right)b_{i,0(u)}\exp\left(\frac{\Delta H_{b(u)}}{RT}\right)p}{1+b_{i,0(u)}\exp\left(\frac{\Delta H_{b(u)}}{RT}\right)p}\right] +$$

$$\frac{p}{p_{PSFTCsm}}\left[k_{Di,0(s)}\exp\left(\frac{\Delta H_{D(s)}}{RT}\right)p + \frac{C'_{Hi,0(s)}\exp\left(\frac{\Delta H_{C(s)}}{RT}\right)b_{i,0(s)}\exp\left(\frac{\Delta H_{b(s)}}{RT}\right)p}{1+b_{i,0(s)}\exp\left(\frac{\Delta H_{b(s)}}{RT}\right)p}\right] \quad (15)$$

In equation (15), $k_{Di,0(u)}$ and $k_{Di,0(s)}$ are the pre exponential Henry's law coefficient, $\Delta H_{D(u)}$ and $\Delta H_{D(s)}$ are the enthalpy of a penetrant molecule in the Henry's law sorbed state, $C'_{Hi,0(u)}$ and $C'_{Hi,0(s)}$ characterizes the pre exponential Langmuir capacity parameter, $\Delta H_{C(u)}$ and $\Delta H_{C(s)}$ are the apparent enthalpy characterizing the temperature dependence of C'_{Hi}, $b_{i,0(u)}$ and $b_{i,0(s)}$ represent the pre exponential Langmuir hole affinity parameter, while $\Delta H_{b(u)}$ and $\Delta H_{b(s)}$ are the enthalpy of penetrant in the Langmuir sorbed state. Subscript (u) and (s) denote unswollen state and swollen states respectively. The parameters are summarized in

Table 6, while prediction to the dual mode sorption behavior over a wide range of operating temperatures is provided in Figure 6 and Figures S2 of Supporting Information.

Table 6 Dual mode sorption parameters as a function of temperature

Parameters	Unswollen	Swollen
$k_{Di,0}$ (cm^3(STP) $cm^{3-1}bar^1$)	5.295×10^{-6}	2.315×10^{-5}
ΔH_D (J/ mol K)	2.672×10^{4}	2.319×10^{4}
$b_{i,0}$ (bar^{-1})	2.148×10^{-1}	1.881×10^{-9}
ΔH_b (J/ mol K)	1.116×10^{4}	4.978×10^{4}
$C'_{Hi,0}$ (cm^3 (STP) cm^{3-1})	2.358×10^{-3}	4.247
ΔH_C (J/ mol K)	1.149×10^{4}	6.024×10^{3}

3.2.1 Glass Transition Temperature

The variations in specific volume versus temperature for unswollen and swollen PSF polymeric membranes at varying operating temperature have been plotted and provided as examples in Figure **7**. In this study, in order to emphasize the findings on operating temperature induced swelling by CO_2 within PSF polymeric membranes as compared to the unswollen state, the evolution change of unswollen structures at different operating temperatures (PSFTC) has been computed, whereby the average value has been reported as reference. In addition, the swollen membrane structures have been treated with the glass transition temperature molecular procedure as highlighted in section 2.2.3 after removal of different number of CO_2 molecules. The alteration in specific volume for swollen PSF membranes at 35 °C, 45 °C and 55°C (PSF35Csm, PSF45Csm and PSF55Csm) has been calculated and tabulated in Figure **7** as well.

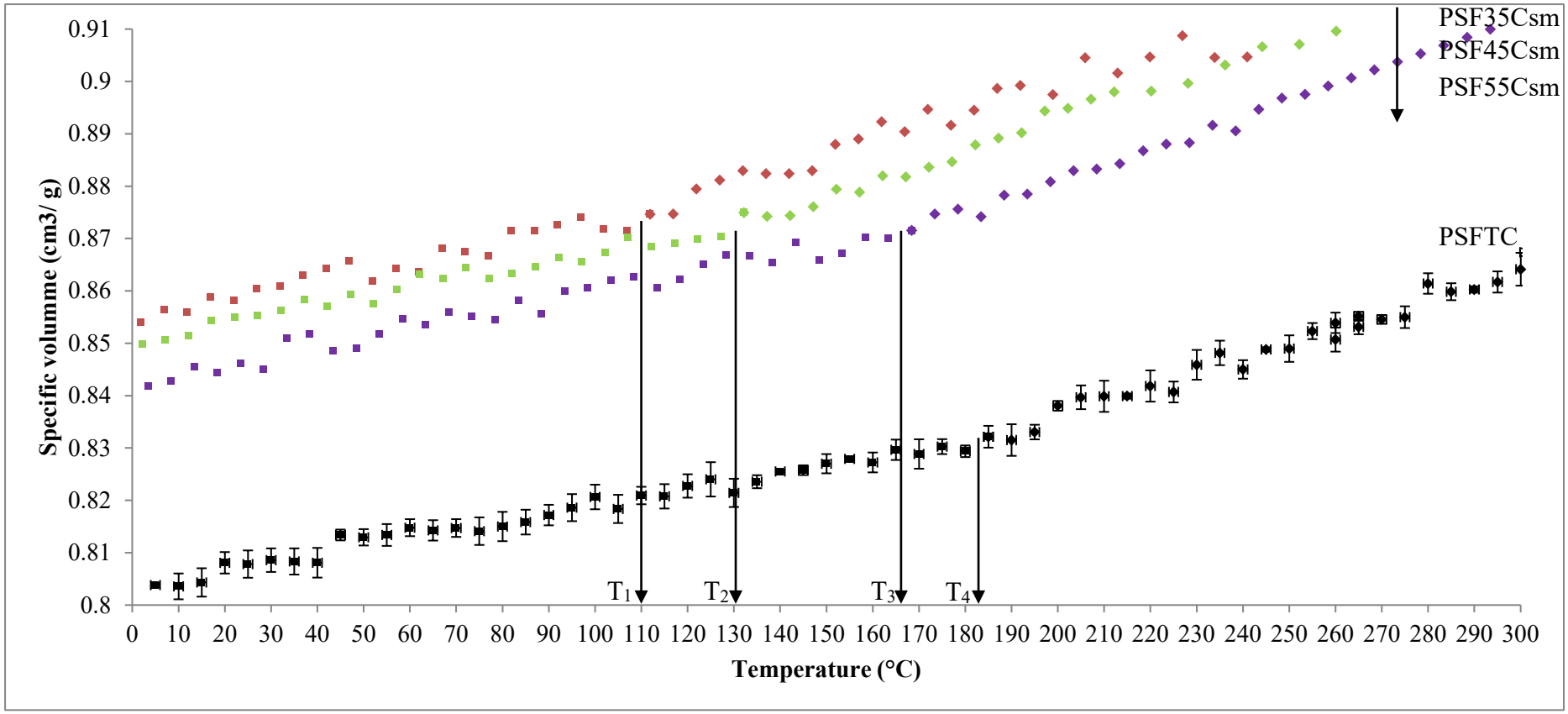

Figure 7 Effect of CO_2 induced swelling at varying operating temperature on specific volume of the polymeric film with respect to alteration in temperature, whereby T_1 (PSF35Csm) = 110.1 °C, T_2 (PSF45Csm) = 132.4 °C, T_3 (PSF55Csm) = 168.2 °C, T_4 (PSFTC) = 184.1 °C, □ specific volume at the glassy state, ◇ specific volume at the reubbery state

As it can be seen from Figure **7**, all the polymeric membranes experience similar behavior with changes in temperature regardless of swelling state. Initially, the specific volume increases linearly with increment in temperature, and then shows an abrupt alteration in the value before continuing to embark in another linear region. Change in linear relationship is demonstrated through the difference in slope between the two curves, whereby the first at lower temperature is representative of the glassy state region, while the latter describes the rubbery state. The point at which the glassy and rubbery linear correlation meets to form an intercept provides graphical representation of the glass transition temperature, T_g. The simulated behavior is consistent to experimental observation reported by Zoller *et al.* (1978), who investigated the pressure-temperature-volume relationships in bulk PSF over a wide range of operating conditions [74]. A T_g of 184.1 °C is obtained from current simulated work for unswollen PSF state. When comparing the obtained T_g through this simulation to literature record of 186 °C [36, 103-105], the error is at -1.02%. The simulated and experimental measured T_g are not significantly different from each other. Thus, it can be proved once again that the proposed methodology is reliable to obtain molecule structures of high accuracy.

Viewing from the effect of CO_2 swelling to T_g, all the swollen structures are demonstrated to inherit a depressed effect in comparison to its unswollen counterpart, which is consistent to measurement of glass transition temperature in actual experimental of swelled polymers [106-108]. The reduction in T_g is typically apparent within the swelled PSF structures exposed to lower operating temperature, in which the T_gs are in the sequence of PSF35Csm < PSF45Csm < PSF35Csm. The observation has been attributed to sorption of higher number of CO_2 within the polymeric matrix when operating temperature is reduced, which consequently enhances the relaxation of polymeric chain within the membrane matrix. The depression in glass transition temperature attributed to enhanced relaxation of polymeric chain is found to be exceptionally evident below operating temperature of 45 °C, which has been supported via the observation of augmented swelling and dilation through membrane specification and physical properties in previous section.

In order to substantiate further understanding towards the relaxation characteristics of the polymeric chains, the mean squared displacement (MSD) has been investigated employing built-in analytical tool located within Materials Studio 8.0, whence the results

have been summarized in Figure 8. Figure 8 (a) shows the MSD for unswollen membrane state, while ΔMSD for swollen membrane (difference in MSD with respect to the reference unswollen state at its designated operating temperature) has been summarized in Figure 8 (b).

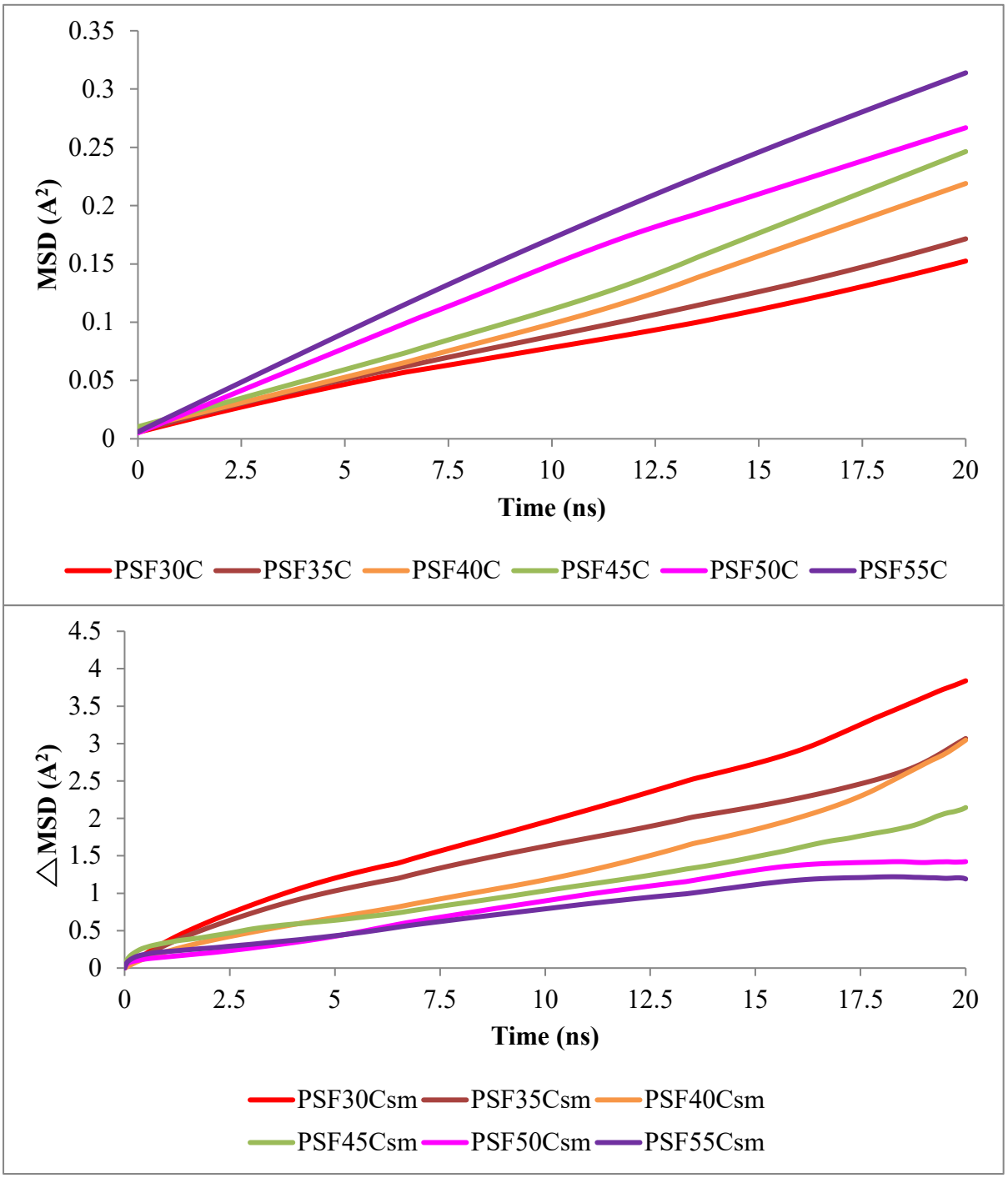

Figure 8 Mean-squared displacements of polymer chains as a function of time in (a) unswollen and (b) swollen PSF at different operating temperatures (Red – 30 °C; Maroon – 35 °C; Orange – 40 °C; Green – 45 °C; Pink – 50 °C; Purple – 55 °C)

From Figure 8, it is found that the MSD of the unswollen membranes in (a) are comparatively lower than its counterpart in (b) at all operating temperatures, which is intuitively reasonable, since no condensable CO_2 gas molecules are included. For unswollen structures in Figure 8 (a), MSD is found to increase with operating temperature, whereby MSD is in the sequence of PSF55C > PSF50C > PSF45C > PSF40C > PSF35C > PSF30C. The enhancement in MSD has been attributed to higher energy state for relaxation with increment in temperature since a smaller MSD indicates confined mobility of the polymeric chains. The MSD of the swollen PSF55Csm, PSF50Csm, PSF45Csm, PSF40Csm, PSF35Csm and PSF30Csm membrane structures are found to exhibit augmented values during the course of molecular treatment in a chronological order, which supported the theoretical claim that interaction between the PSF polymeric chain and CO_2 contributes to ease of movement for chain molecules to slip over one another and thus causing polymer softening [19, 20]. As the number of CO_2 loading increases within the swelled structures from 55°C to 30°C, the mobility has been enhanced, which has been proven through the higher MSD pattern. Similarly, the MSD behaviour within the PSF45Csm, PSF40Csm, PSF35Csm and PSF30Csm membranes are found to increase in a considerable significant manner with time as compared to the PSF55Csm and PSF50Csm structures, which is consistent to the observation of enhanced depression in glass transition temperature in these molecular structures, such as that demonstrated in Figure 7. The MSD pattern further confirms the theory that dilation attributed to operating temperature is less vital in determining the relaxation since the MSD at higher operating temperature starts off with a higher value at the unswollen condition, but further exhibits the least deviation from the reference unswelled state since it has the least number of CO_2. The simultaneous effect of operating temperature and CO_2 concentration under the swollen state confirms that concentration parameter is the more prevailing factor in swelling phenomena.

3.2.2 Free Volume

In this section, the free volume within the unswollen and swollen PSF membranes at varying operating temperatures have been elucidated through adaptation of procedure as highlighted in section 2.2.3. Figure **9** depicts examples of simulated cell for pure PSF at the unswollen and swollen states of different operating temperature.

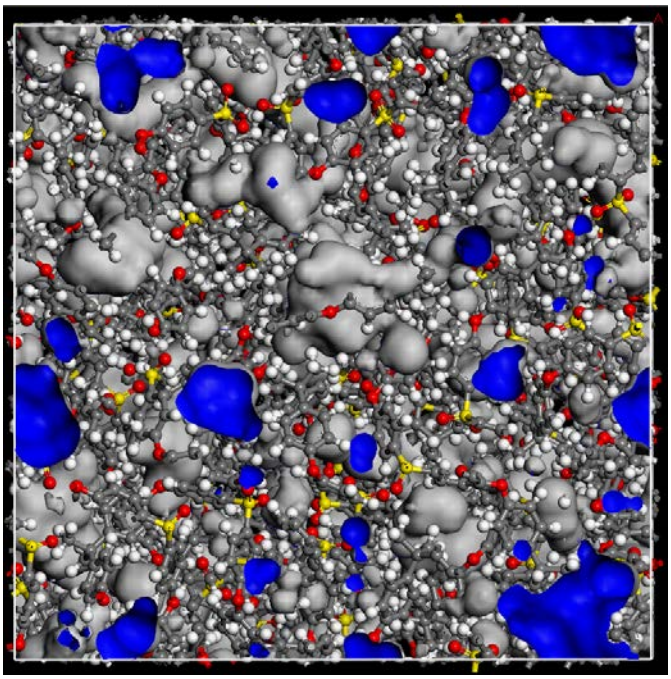

PSF35C

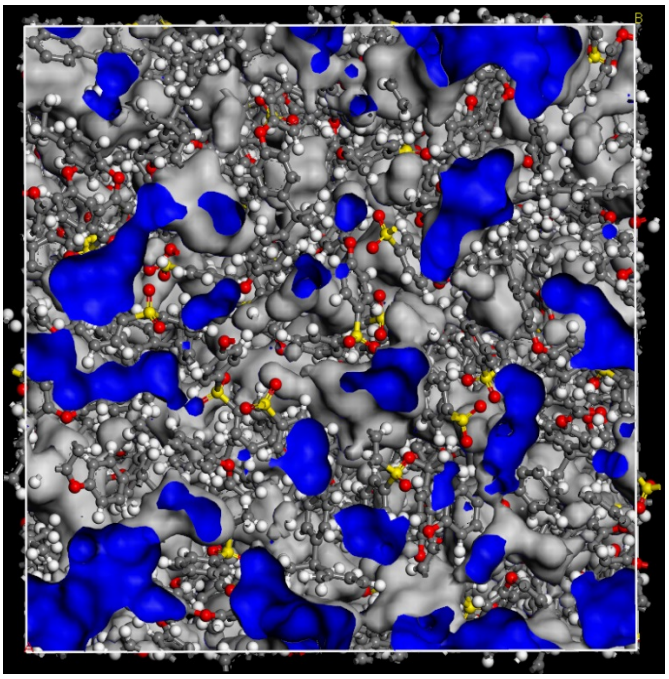

PSF30Csm

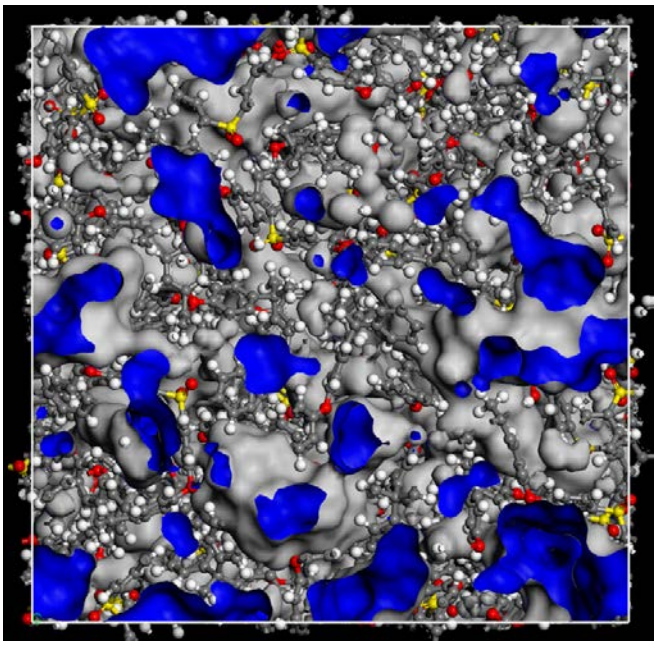

PSF35Csm

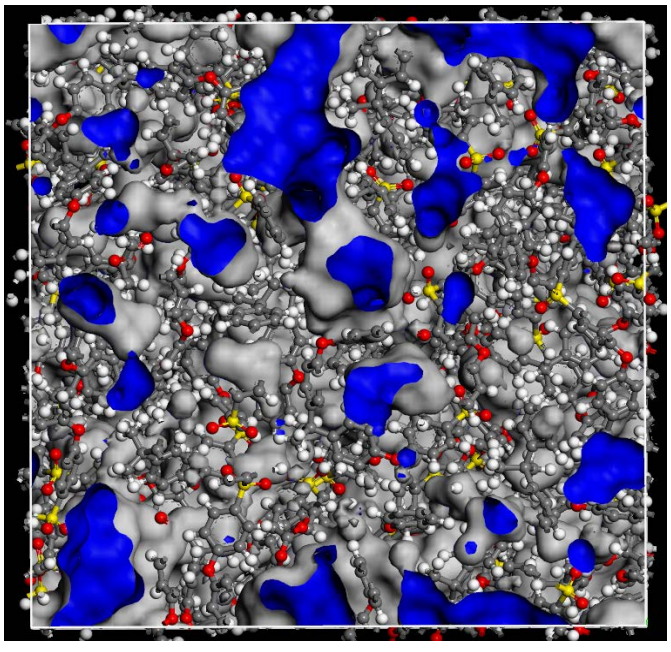

PSF40Csm

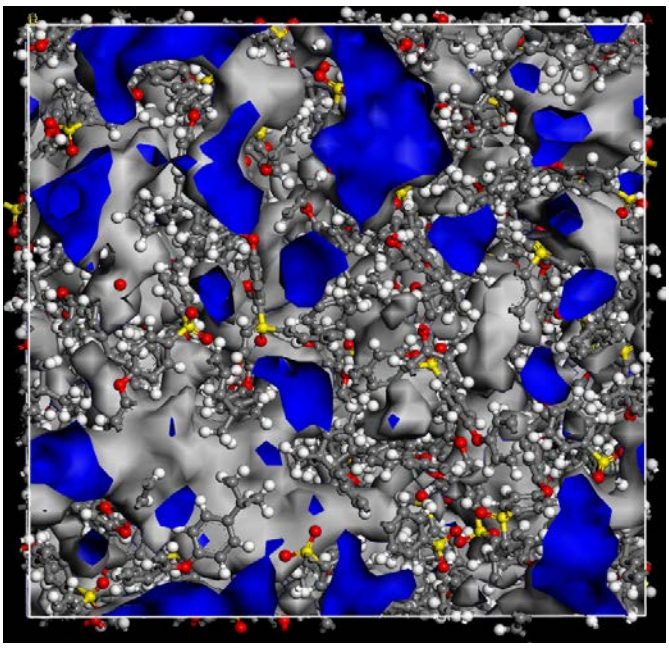

PSF45Csm

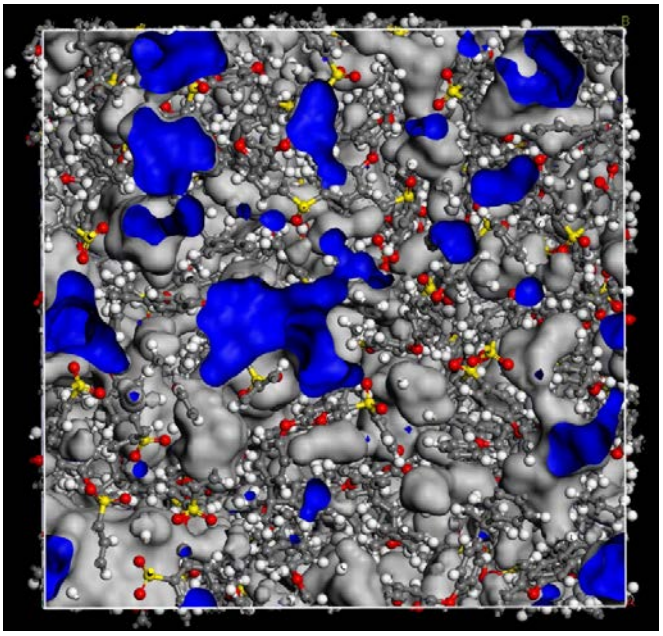

PSF50Csm

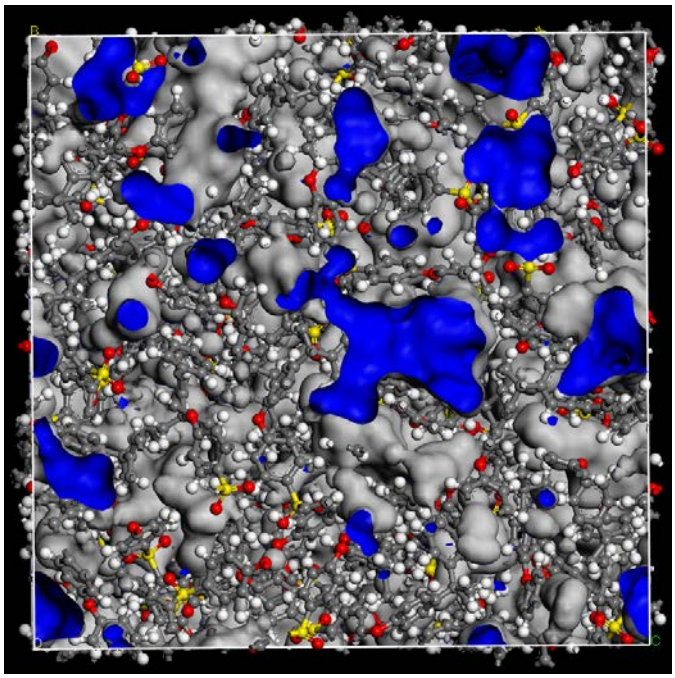

PSF55Csm

Figure 9 2 dimensional view for simulation cells of unswollen and swollen PSF membranes at different operating temperature, the grey indicates the occupied region of polymeric chains while the blue characterizes those of the free space

As shown in Figure 9, the ratio of blue to grey area is found to be increasing for swollen as compared to the unswollen membrane structures, and with decrement in operating temperature for swollen amorphous cell, in which the sequential blue to grey proportion is in the order of PSF35C < PSF55Csm < PSF50Csm < PSF45Csm < PSF40Csm < PSF35Csm < PSF30Csm. This phenomenon has been rationalized through enhanced mobility of PSF polymeric chains in the vicinity of CO_2 gas molecules, whereby the sorbed CO_2 swells the polymeric matrix, which further contributes to volume dilation and more free space within the membrane. By employing Connolly Surface module in Materials Studio and a probe radius of 1.8 Å, the occupied, free and total volume of each PSF structure are conveniently computed, which have been adopted to calculate the FFV (MS) and summarized in Table 7. Similarly, FFV (Bondi) has been computed and tabulated in Table 7 as well to provide comparison with FFV (MS).

Table 7 Free volume characteristic of simulated unswollen and swollen Polysulfone membranes at different operating temperature

Operating temperature (°C)	Unswollen model (PSFTC)				Swollen model (PSFTCsm)			
	Occupied Volume (Å^3)	Free Volume (Å^3)	FFV (MS)	FFV (Bondi)	Occupied Volume (Å^3)	Free Volume (Å^3)	FFV (MS)	FFV (Bondi)
30	47686.28	8021.67	0.1440	0.1459	47541.10	11956.04	0.2010	0.1991
35	47737.14	8150.42	0.1458	0.1468	47965.00	11509.28	0.1990	0.1983
40	47515.09	8313.91	0.1489	0.1477	47743.09	11630.68	0.1959	0.1968
45	47470.38	8419.12	0.1506	0.1486	47797.77	11475.61	0.1936	0.1955
50	47369.55	8580.45	0.1534	0.1496	47910.31	11058.03	0.1875	0.1913
55	47217.83	8792.67	0.1570	0.1505	47984.38	10879.49	0.1848	0.1899

FFV deduced from the Bondi's manner demonstrates a remarkably similar trend with the effect of operating temperature on CO_2 induced swelling found through FFV of Materials Studio, which confirms applicability of the methodology. The good accordance in trending stimulates further adaptation of the methodology to determine quantitative analysis of polymeric membrane free volume in material mathematical modelling in future work. In an overall, the FFVs demonstrate an increment with decrement in operating temperature, attributed to the amplified sorption of CO_2 gas molecules, while the pristine PSF membrane has the lowest FFV value.

The observation of cavity size distribution is consistent to those observed through molecular simulation work as summarized in Figure **9**. As depicted in Figure **9**, the blue areas in the unswollen PSF35C structure are agglomerated into smaller individual cavities, while that of swollen PSF30Csm, PSF35Csm, PSF40Csm, PSF45Csm, PSF50Csm and PSF55Csm are found to inherit bigger and more continuous characteristics. Nonetheless, the agglomeration of blue areas is found to be typically prominent within the molecular structure less than 45 °C. The observation of larger void elements in PSF polymeric membranes with packing of CO_2 gas molecules have been rationalized through swelling induced effect, whence presence of CO_2 that interacts with the polymeric chains causes insufficient polymer chain packing. In other words, the polymeric chains are packed less efficiently and more sparsely with respect to one another, subsequently contributes to formation of bigger cavity sizes. At lower operating temperature, the tendency of CO_2 to be absorbed within the polymeric membrane matrix is higher, constituting to the inhabitancy of a larger number of CO_2 that contributes to enhanced relaxation effect that induces larger free channels along the polymeric chains. Typically when the concentration of CO_2 exceeds the threshold of critical concentration, the dilation effect becomes more prominent, evident through larger and more continuous channels and void spaces.

3.2.3 Radial Distribution Function

The radial distribution functions (RDFs) can be employed to acquire an in-depth analysis of interaction between a certain gas penetrant and polymeric chain within the membrane matrix. Theoretically, the accessibility and affinity of a gas species within the membrane matrix can be evaluated based on the location and intensity of the peaks in RDF, with a shorter distance and higher peak resembling greater interaction between the gas

molecules and functional group of polymeric chain. The RDF has been determined conveniently through embedded analytical tool located within Forcite module of Materials Studio. Through the software, the RDF, $g_{P-CO_2}(r)$, represents the probability of finding a pair of CO_2 molecule at a distance r with respect to the bulk polymer, P, phase in a completely random distribution, whereby the definition is provided in Eq. (16).

$$g_{P-CO_2}(r) = \frac{1}{\rho_{P-CO_2} 4\pi r^2} \frac{\sum_{t=1}^{K} \sum_{j=1}^{N_{P-CO_2}} \Delta N_{P-CO_2}(r \to r+\delta r)}{N_{P-CO_2} \times K} \quad (16)$$

In Eq. (16), N_{P-CO_2} is the total number of polymer molecules, P, and CO_2 in the system, K the number of time steps, δr the distance interval, ΔN_{P-CO_2} the number of CO_2 (or P) molecules between $r + \delta r$ around a P (or CO_2) molecule, and ρ_{P-CO_2} the bulk density. In this work, the RDF of CO_2 around three typical atoms of the PSF repeat unit is investigated, typically oxygen in the sulfone functional group, carbon in the methyl group and oxygen in the ether group, denoted as O1, C1 and O2 respectively, such as that depicted in Figure 1. The results pertaining to the RDF that characterizes interaction between varying functional groups in PSF and CO_2 gas molecules are provided in Figure 10.

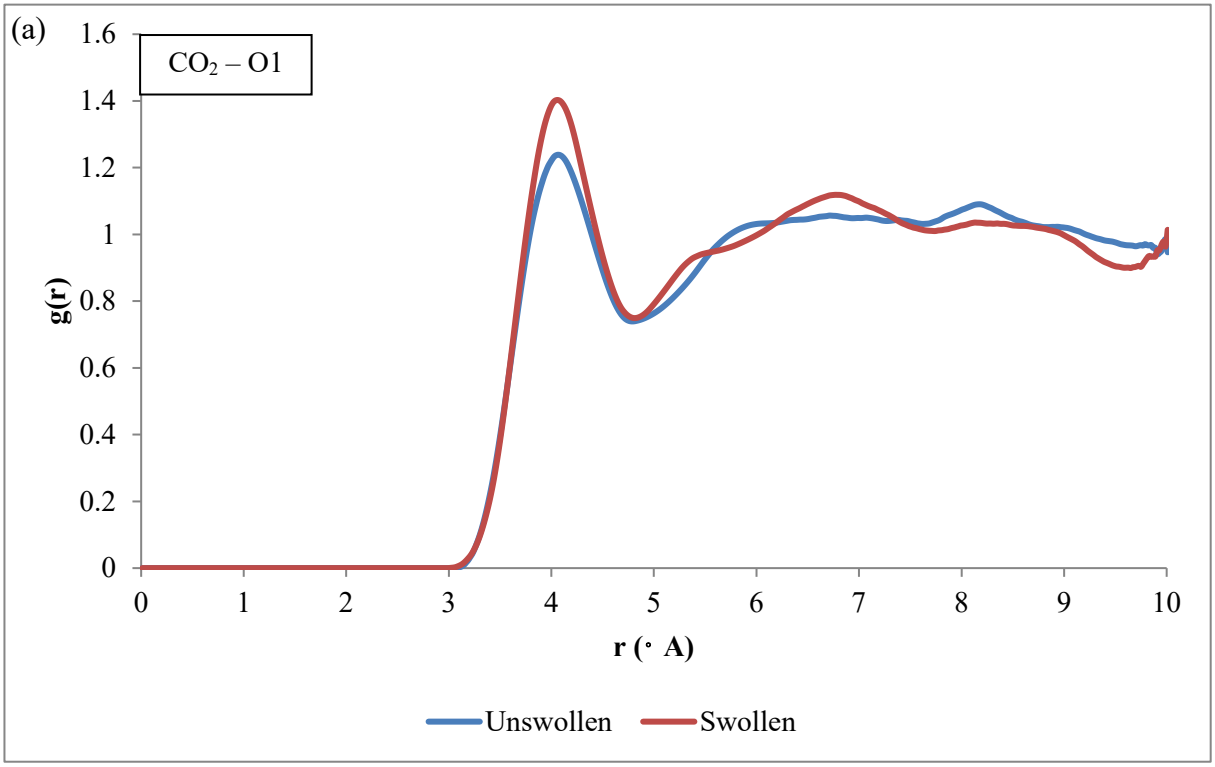

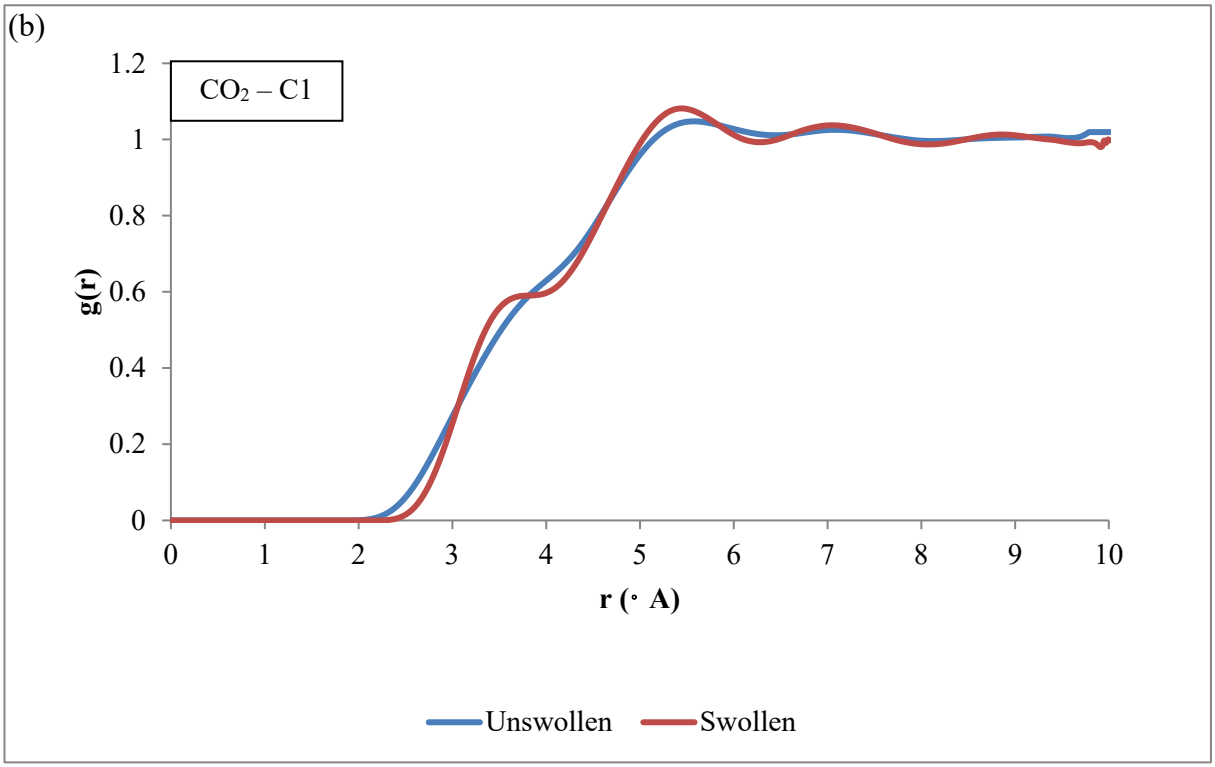

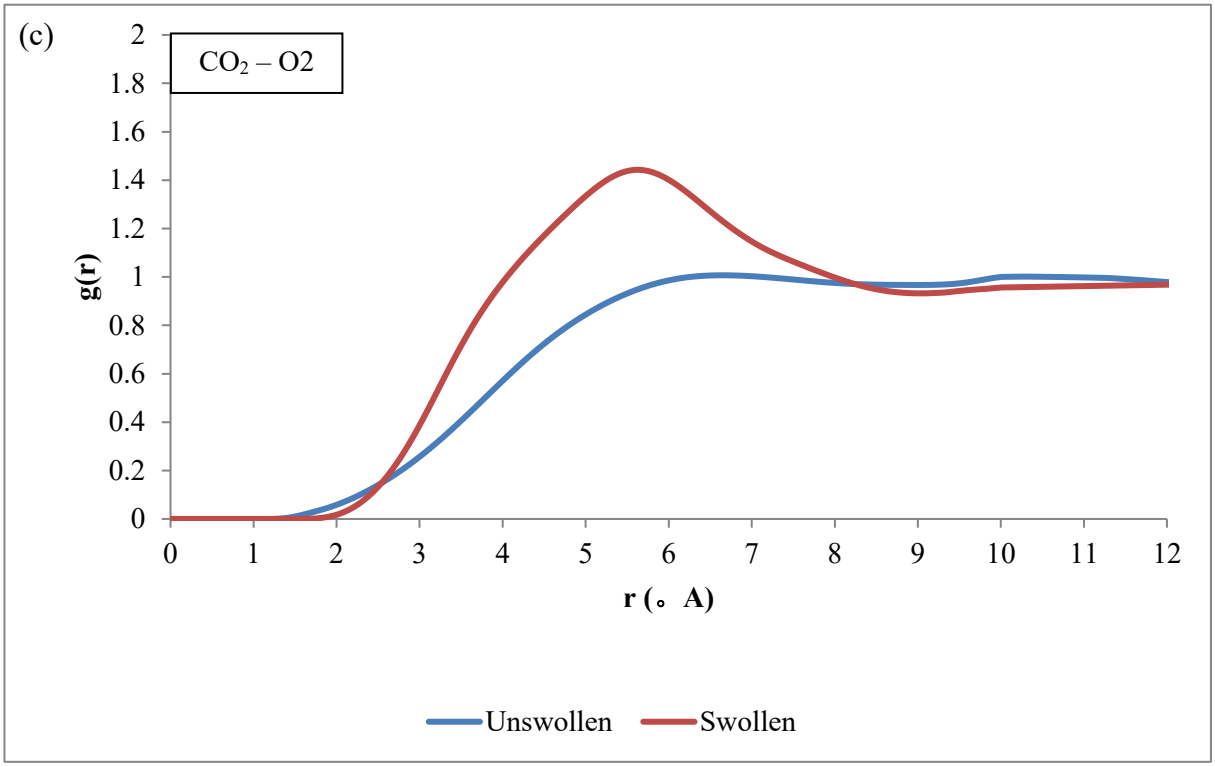

Figure 10 Radial distribution function g(r) of CO_2 around (a) O1 (b) C1 and (c) O2 atoms respectively in unswollen polysulfone (PSF35C) and swollen PSF at operating temperature of 35 °C (PSF35sm)

From Figure 10, for unswollen PSF membrane structure, peaks are observable in the g(r) of CO_2 – O1 at ~ 4 Å in (a), which indicates that the O1 of sulfone groups are preferential sorption sites for CO_2. The atoms that are highly accessible have been postulated to exhibit specific interaction with CO_2 (e.g. hydrogen bonding or Lewis acid–base complex formation) [109-111]. Nonetheless, no distinct peak is distinguished in g(r) of CO_2 – C1 and CO_2 – O2, which is represented in Figure 10 (b) and (c). The C1 site has minimal interaction with CO_2, which can be rationalized through the bulky methyl group that constitutes to creation of local voids, whereby potential field is not sufficiently strong enough that hinders the accessibility to CO_2 [18]. On the other hand, the O2 sorption sites is not highly attractive to CO_2 gas penetrants since they are restricted between two phenyl rings, which confine their availability to sorbate molecules.

For swollen PSF membrane structure, similar behavior has been clearly seen for the g(r) characterizing interaction of CO_2 – O1, whereby prominent peak is seen at ~4 Å in Figure 10 (a). The peaks of these sorption sites are considerably higher than its counterpart at the unswollen state attributed to higher concentration of CO_2 in the swollen structure. Viewing from the aspect of g(r) of CO_2 – C1, no apparent peak has been observed for the swollen PSF membrane structure. The observation has been attributed to the bulky methyl group that constitutes to great impediment for CO_2 sorbates to access it as elaborated earlier. As for CO_2 – O2 functional group, a clear peak is seen for the swollen membrane structure at ~5.5 Å, which indicates that the O2 ether group demonstrates binding affinity with CO_2 as compared to the pristine PSF membrane. The distinction in g(r) between the unswollen and swollen PSF membrane suggests that interaction between CO_2 and O2 atom in the ether group is responsible upon onset of enhanced dilation observed. The lone pair electrons in the O2 ether are coupled with the inter-segmental phenyl rings, whereby the charge transfer with the phenyl rings is reduced with occupation of CO_2 gas molecules. As a result, the oxygen-phenyl ring bond inherits a more favorable rotational characteristic, which consequently leads to less intersegment rigidity and more flexible polymeric chains, further minimizing the steric hindrance for CO_2 to reach the ether oxygen and hence enhanced relaxation behavior.

3.2.4 Quantification of Specific Interaction between CO_2 and Polymer Chain

In this section, the specific interaction between CO_2 and PSF polymeric chain has been quantified through proposal of associating relationship between the two, whereby the reversible equation governing the process is presented in (17).

$$\mu CO_2 + P <=> P \ldots (CO_2)_\mu \quad (17)$$

In (17), μ is the CO_2/ polymer binding ratio, CO_2 is the plasticizer, P is the polymer segment and $P \ldots (CO_2)_\mu$ is the polymer-CO2 complex that is formed during the association reaction. The equilibrium constant, K_{eq}, for the aforementioned chemical reaction is given by Eq. (18).

$$K_{eq} = \frac{[P \ldots (CO_2)_\mu]}{[P][CO_2]^\mu} \quad (18)$$

For a system containing xN_p polymer segments, whereby x is the number of repeat unit of the polymer chain, and N_{CO_2} solvent molecules, of which $n_{P-CO_2}(r_c)$are associated, which is the coordination number of P and CO_2 molecules, the equilibrium constant is translated to the following in Eq. (19).

$$K_{eq} = \frac{\left[\frac{n_{P-CO_2}(r_c)}{N_{CO_2}+xN_p-n_{P-CO_2}(r_c)}\right]}{\left[\frac{xN_p-n_{P-CO_2}(r_c)}{N_{CO_2}+xN_p-n_{P-CO_2}(r_c)}\right]\left[\frac{N_{CO_2}-n_{P-CO_2}(r_c)}{N_{CO_2}+xN_p-n_{P-CO_2}(r_c)}\right]^\mu} \quad (19)$$

The coordination number of P and CO_2 molecules, $n_{P-CO_2}(r_c)$, can be integrated from the radial distribution function pattern, in which r_c can be assumed to be the minimum after the peak in RDF that characterizes the commencement of distance, whereby the $P - CO_2$ interaction becomes insignificant, such as that shown in Eq. (20).

$$n_{P-CO_2}(r_c) = \frac{N_{P-CO_2}}{v_{cell}} \int_0^{r_c} g_{P-CO_2}\, 4\pi r^2 dr \quad (20)$$

In present study, the RDF has been integrated by computing area under the curve via employment of numerical integration (trapz) in Matlab® 2013.

As such, K_{eq}, can be characterized through a temperature dependent correlation described by Van 't Hoff , as shown in Eq. (21) [112].

$$ln\frac{K_{eq}}{K_{eq}^*} = \frac{-\Delta H_{P,CO2}}{R}\left(\frac{1}{T} - \frac{1}{T^*}\right) \quad (21)$$

In Eq. (21), K_{eq}^* describes the equilibrium constant for association at a specific reference temperature, T^*, while $\Delta H_{P,CO2}$ represents the enthalpy of association. In the above expression, $\Delta H_{P,CO2}$ has been assumed to be independent of T over the range of temperature

of interest. Therefore, by determining K_{eq} at several operating temperatures, Ts, $\Delta H_{P,CO2}$ can be calculated and subsequently be employed to predict K_{eq} that characterizes the extend of interaction between CO_2 and polymer at a different temperature of interest.

The RDF of CO_2 around O2 atoms of ether group in molecular structures of PSF30Csm, PSF35Csm, PSF40Csm and PSF45Csm has been provided in Figure 11.

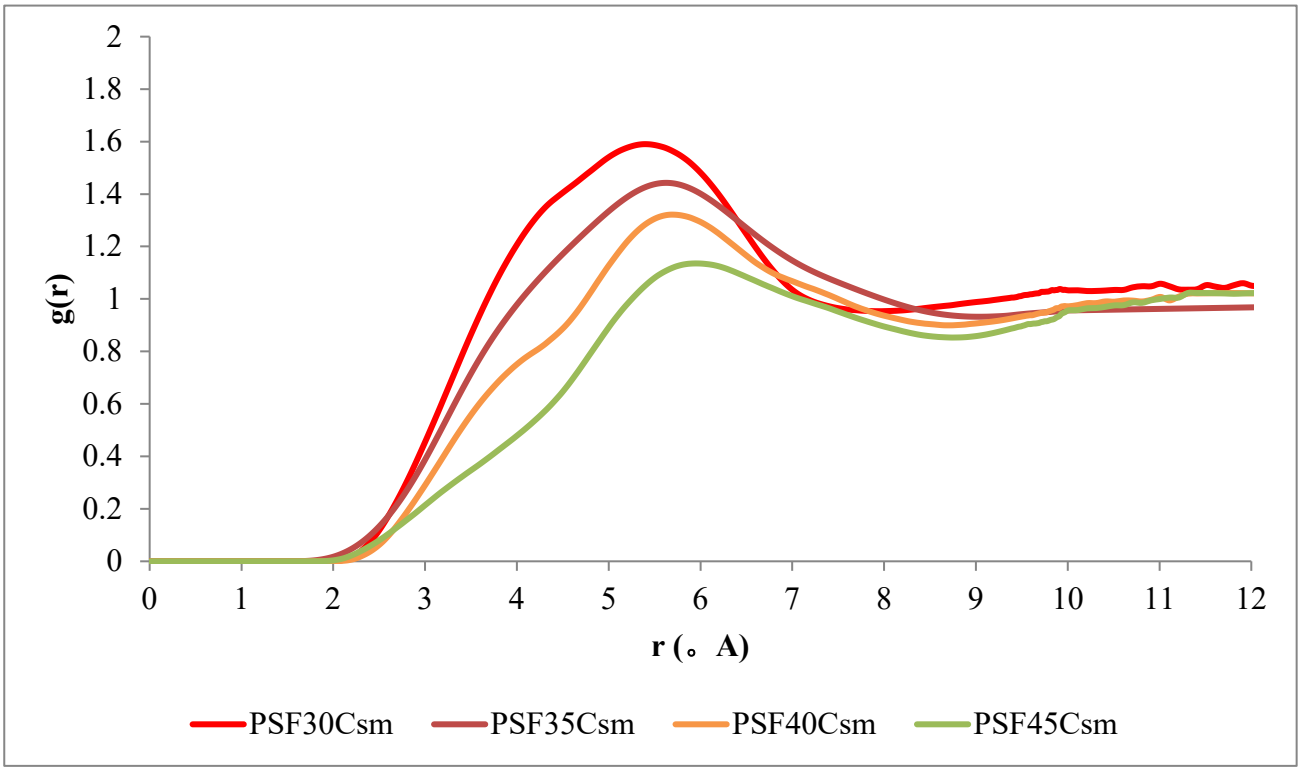

Figure 11 Radial distribution function g(r) of CO_2 around O2 atoms of ether group in PSF30Csm, PSF35Csm, PSF40Csm and PSF45Csm respectively

It has to be noted that no distinct peak has been observed for molecular structures of PSF50Csm and PSF55Csm between the RDF of CO_2 and O2 atoms of ether group, whereby the only peak is merely noticeable at ~ 4 Å with O1 atoms of the sulfone group within the polymeric chain backbone. The RDF in PSF50Csm and PSF55Csm has been provided in Figure S3 of Supplementary Information. From the RDF, it can be concluded that the lower sorption of CO_2 at higher operating temperature causes the invisibility of peaks in O2 atoms of ether group since all the sorbed CO_2 occupy the favourable sites of O1 sulfone group. With increment in the number of CO_2 sorbates, the favourable sites become saturated and start to attack the less preferential groups, such as C1 and O2 in present study, which contributes to

lower peaks in CO_2 and O1 sulfone group in PSF35Csm membrane structure in Figure 10 as compared to PSF50Csm and PSF55Csm in Figure S3. It has been hypothesized the interaction between CO_2 and O2 ether group contributes to augmented swelling and dilation effect, which is only observable within molecular structures of PSF30Csm, PSF35Csm, PSF40Csm and PSF45Csm. The enhanced dilation due to the ether group contributes to increment in void passages that may constitute to increment in gas permeability of all gas species with pressure, which is known as plasticization. Under this condition, the ability of polymeric material to sieve gas molecules for permeation becomes weaker and hence causes reduction in selectivity. This hypothesis requires more study and evident to support the claim, typically those involving gas transport properties, and shall be dealt with in a subsequent publication.

From Figure 11, it is found that the RDF at 30 °C demonstrates a higher and broader peak spectrum in comparison to the other structures at higher operating temperature attributed to a larger number of sorbed CO_2 gas molecules that exhibit greater interaction with the polymeric chain. Intuitively, the molecular structure with a greater CO_2 loading at lower operating temperature demonstrates a greater K_{eq} value. Viewing from the aspect of plot of $\ln K_{eq}$ versus $1/T$ in

Figure **12**, a relatively linear correlation with a good fit (R^2 = 0.9848) has been obtained.

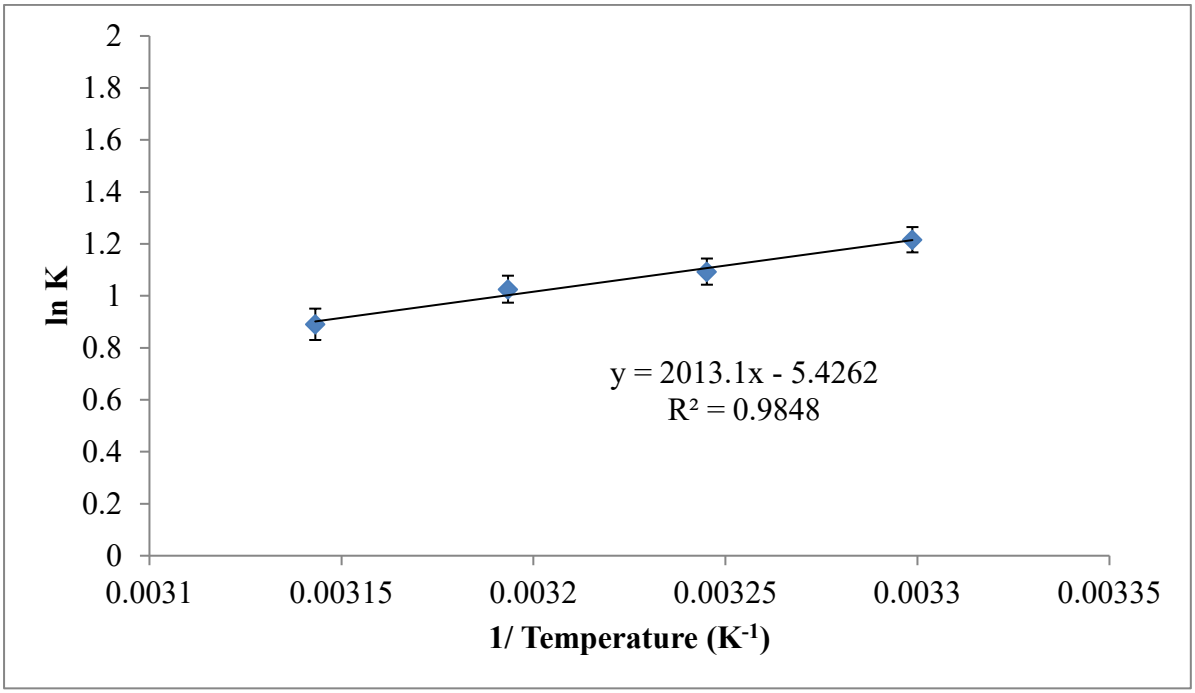

Figure 12 Linear plot of ln K_{eq} versus 1/ T

From slope of the linear relationship, a $\Delta H_{P,CO2}$ of -16.74 kJ/ mol has been computed based on present study. This value is found to be in good compliance with published literature by Kilic *et al.* (2007), who reported interaction energies of ether group with CO_2 to be from the range of -14.8 to -18.6 kJ/ mol in varying chemical structures [113]. The satisfactory accordance demonstrates that the proposed methodology in present study is of sufficient accuracy to characterize specific interaction between CO_2 and functional groups of polymeric chain. This study demonstrates that the findings of atomistic behaviour at a microscopic scale can be extended to extrapolation of material properties applied to new applications and operation windows at a macroscopic level [114-116], which emphasizes the importance of molecular modelling in present study.

4. Conclusion

In current work, molecular simulation has been conducted to construct unswollen and swollen polysulfone membranes at different operating temperatures in accordance to input from actual experimental measurement and conditions. Accuracy of the developed molecular structures has been validated with experimental measured physical property and in-house experimental set up for sorption measurement of gas molecules within polysulfone membrane, whereby only a small deviation between simulation prediction and experimental measurement has been observed. The developed molecular structures have been employed to elucidate the effect of operating temperature to CO_2 induced dilation within polysulfone membrane to determine the most dominant parameter that governs swelling phenomena since in-situ observation at the laboratory scale is costly and nearly impossible. For unswollen polymeric membranes, it is found to demonstrate enhanced relaxation characteristic with increment with temperature, such as greater cell dimension, lower density of the membrane matrix and greater MSD. The swollen structure is found to exhibit dilated characteristic demonstrated through, depression in glass transition temperature and bigger free volume as compared to the pristine unswollen polysulfone membrane. Nonetheless, the effect of CO_2 induced swelling is found to be typically substantial within molecular structure at lower operating temperature (PSF30Csm > PSF35Csm > PSF40Csm > PSF45Csm > PSF50Csm > PSF45Csm) since the CO_2 gas molecules has a higher affinity to be sorbed within the polymeric matrix. The CO_2 gas molecules interact with the polymeric chain, which

contributes to enhanced relaxation effect as end effect, which further surpasses the effect of operating temperature. Through elucidation of radial distribution function between CO_2 and functional groups within the polysulfone polymeric chain, it is found that interaction of CO_2 with the oxygen ether group is in charge of the augmented swelling, whence CO_2 causes the oxygen-phenyl ring bond to inherit a more favourable rotational characteristic and therefore augmented dynamics of the polymer. In PSF50Csm and PSF55Csm molecular structures, whereby the CO_2 has a lower affinity to be condensed within the polymeric membrane matrix and does not exceed a certain critical concentration, interaction of CO_2 with ether group of PSF polymeric chain is not evident, which explains the dilation but at much smaller extend in comparison to their counterpart at lower operating temperatures. Finally, a series of association equations has been proposed to quantify the specific energy of interaction between CO_2 and ether group of polysulfone, whereby a value of -16.74 kJ/ mol has been computed from present study. It is expected that the findings from current work can be sufficiently employed to overcome the barrier, cost and time in preparation and testing of gas permeation in membrane at the laboratory scale to predict CO_2 swelling phenomena since it appears to be relatively convenient and straightforward to control operating conditions of the simulation.

Acknowledgement

This work is done with the financial support from Universiti Teknologi PETRONAS.

Abbreviation

n_1	Amount of gas presents in the reservoir chamber
V_{C1}	Inner volume of the reservoir chamber
P_1	Pressure of gas introduced into reservoir chamber
n_{1+2}	Amount of gas residing in reservoir and membrane chamber after equilibration
V_{C2}	Inner volume of the membrane chamber
P_2	Equilibration pressure when membrane sample is saturated
Z_1, Z_2	Compressibility factor of the real gas under the designated operating condition, P_1 and T, and P_2 and T respectively

V_s	Volume of the polymeric sample
n_p	The amount of gas dissolved into the polymeric sample
T	Temperature of the system
x	The concentration of gas molecule sorbed within the polymer membrane
V_p	Volume of the polymer sample in the membrane chamber
$\bar{n}$	Refractive index of the polymer sample
ρ_p	Density of the polymer sample
N_{av}	Avogadro's number
$\bar{\alpha}$	Average polarizabiliy of the i^{th} type chemical bond, which is dependent upon the wavelength parameter
k_i	Number of such bonds per repeat unit of polymer
M_0	Molecular weight of the polymer repeat unit
ε_0	Permittivity constant of free space
C	Material constant that relates refractive index to polymer density
n_{sim}	Number of CO_2 loading taken from sorption experiment in present work
v_{cell}	Volume of simulation box in Materials Studio
T_g	Glass transition temperature
FFV	Fractional free volume
v_g	Specific volume of polymeric glass at a specific temperature
v_o	Occupied volume of polymeric chain
$(v_w)_k$	Van der Waals volume of each group into which a polymeric chain is divided
C_i	Total concentration of gas i in a polymer matrix
C_{Di}	Equilibrium population of gas i existing in the polymer matrix under the dissolved mode and is governed by Henry's Law equation
C_{Hi}	Non-equilibrium population of gas i existing in excess within the hole-filling environment governed by Langmuir parameters
k_{Di}	Henry's law coefficient that characterizes dissolution of gas i in the polymer
b_i	Langmuir hole affinity parameter of gas i in the polymer

C'_{Hi}	Capacity parameter of gas i in the polymer
f_i	Fugacity of gas i in the system
$\langle y \rangle$	Average cavity size
y	Cavity size
P(v)	Probability distribution of cavity sizes
P	Polymer segment
CO_2	Carbon dioxide plasticizer
$g_{P-CO_2}(r)$	Probability of finding a pair of CO_2 molecule at a distance r with respect to the bulk polymer, P, phase in a completely random distribution
N_{P-CO_2}	Total number of polymer molecules, P, and CO_2 in the molecular system
K	Number of time steps
δr	Distance interval
ΔN_{P-CO_2}	Number of CO_2 (or P) molecules between $r + \delta r$ around an P (or CO_2) atom
ρ_{P-CO_2}	Bulk density of the polymer, P, and CO_2 system
μ	CO_2/ polymer binding ratio
$P \ldots (CO_2)_\mu$	Polymer-CO_2 complex that is formed during the association reaction
K_{eq}	Equilibrium constant of polymer-CO_2 association reaction
N_p	Number of polymer segments
N_{CO_2}	Number of CO_2 solvent molecules
x	Number of repeat unit of the polymer chain
$n_{P-CO_2}(r_c)$	The coordination number of P and CO_2 molecules
K_{eq}^*	Equilibrium constant for association at a specific reference temperature, T^*
$\Delta H_{P,CO2}$	The enthalpy of association of polymer-CO_2 reaction

Reference

[1] X. He, M.-B. Hägg, T.-J. Kim, Hybrid FSC membrane for CO2 removal from natural gas: Experimental, process simulation, and economic feasibility analysis, AIChE J. 60(12) (2014) 4174-4184.

[2] J. Marriott, E. Sørensen, A general approach to modelling membrane modules, Chem. Eng. Sci. 58(22) (2003) 4975-4990.

[3] H.J. Jung, S.H. Han, Y.M. Lee, Y.-K. Yeo, Modeling and simulation of hollow fiber CO2 separation modules, Korean J. Chem. Eng. 28(7) (2011) 1497-1504.

[4] S.S.M. Lock, K.K. Lau, F. Ahmad, A.M. Shariff, Modeling, simulation and economic analysis of CO2 capture from natural gas using cocurrent, countercurrent and radial crossflow hollow fiber membrane, Int. J. Greenh. Gas Control 36 (2015) 114-134.

[5] A.S. Gh, A.H. Navarchian, Matrimid–polyaniline/clay mixed-matrix membranes with plasticization resistance for separation of CO2 from natural gas, Polym. Adv. Technol 27(9) (2016) 1228-1236.

[6] D.F. Mohshim, H. Mukhtar, Z. Man, R. Nasir, Latest Development on Membrane Fabrication for Natural Gas Purification: A Review, J. Eng. 2013 (2013) 7.

[7] D. Bastani, N. Esmaeili, M. Asadollahi, Polymeric mixed matrix membranes containing zeolites as a filler for gas separation applications: A review, J. Ind. Eng. Chem. 19(2) (2013) 375-393.

[8] Y.P. Handa, S. Capowski, M. O'Neill, Compressed-gas-induced plasticization of polymers, Thermochim. Acta 226 (1993) 177-185.

[9] P. Pissis, L. Apekis, C. Christodoulides, M. Niaounakis, A. Kyritsis, J. Nedbal, Water effects in polyurethane block copolymers, J. Polym. Sci. Pt. B Polym. Phys. 34(9) (1996) 1529-1539.

[10] R.M. Hodge, T.J. Bastow, G.H. Edward, G.P. Simon, A.J. Hill, Free Volume and the Mechanism of Plasticization in Water-Swollen Poly(vinyl alcohol), Macromol. 29(25) (1996) 8137-8143.

[11] K.-I. Okamoto, N. Tanihara, H. Watanabe, K. Tanaka, H. Kita, A. Nakamura, Y. Kusuki, K. Nakagawa, Sorption and diffusion of water vapor in polyimide films, J. Polym. Sci. Pt. B Polym. Phys. 30(11) (1992) 1223-1231.

[12] B.-G. Wang, T. Yamaguchi, S.-I. Nakao, Solvent diffusion in amorphous glassy polymers, J. Polym. Sci. Pt. B Polym. Phys. 38(6) (2000) 846-856.

[13] B.J. Briscoe, C.T. Kelly, The effect of structure on gas solubility and gas induced dilation in a series of poly(urethane) elastomers, Polym. 37(15) (1996) 3405-3410.

[14] J.D. Wind, D.R. Paul, W.J. Koros, Natural gas permeation in polyimide membranes, J. Membr. Sci. 228(2) (2004) 227-236.

[15] H.B. Park, C.H. Jung, Y.M. Lee, A.J. Hill, S.J. Pas, S.T. Mudie, E. Van Wagner, B.D. Freeman, D.J. Cookson, Polymers with Cavities Tuned for Fast Selective Transport of Small Molecules and Ions, Sci. 318(5848) (2007) 254-258.

[16] H. Lin, E. Van Wagner, B.D. Freeman, L.G. Toy, R.P. Gupta, Plasticization-Enhanced Hydrogen Purification Using Polymeric Membranes, Sci. 311(5761) (2006) 639-642.

[17] M.S. Suleman, K.K. Lau, Y.F. Yeong, Plasticization and Swelling in Polymeric Membranes in CO2 Removal from Natural Gas, Chem. Eng. Techol. 39(9) (2016) 1604-1616.

[18] L. Zhang, Y. Xiao, T.-S. Chung, J. Jiang, Mechanistic understanding of CO2-induced plasticization of a polyimide membrane: A combination of experiment and simulation study, Polym. 51(19) (2010) 4439-4447.

[19] M.R. Coleman, W.J. Koros, Conditioning of Fluorine Containing Polyimides. 1. Effect of Exposure to High Pressure Carbon Dioxide on Permeability, Macromol. 30(22) (1997) 6899-6905.

[20] M.R. Coleman, W.J. Koros, Conditioning of Fluorine-Containing Polyimides. 2. Effect of Conditioning Protocol at 8 Volume Dilation on Gas-Transport Properties, Macromol. 32(9) (1999) 3106-3113.

[21] A.L. Ahmad, J.K. Adewole, C.P. Leo, S. Ismail, A.S. Sultan, S.O. Olatunji, Prediction of plasticization pressure of polymeric membranes for CO2 removal from natural gas, J. Membr. Sci. 480 (2015) 39-46.
[22] M. Alcoutlabi, G.B. McKenna, Effects of confinement on material behaviour at the nanometre size scale, J. Phys. Condens. Matter 17 (2005) R461-R524.
[23] N. Hedin, L. Chen, A. Laaksonen, Sorbents for CO2 capture from flue gas-aspects from materials and theoretical chemistry, Nanoscale 2(10) (2010) 1819-1841.
[24] R. Krishna, J.M. van Baten, A Molecular Dynamic Investigation of the Diffusion of Methane-Ethane and Methane-Propane Mixtures in Zeolites, Chem. Eng. Techol. 29(12) (2006) 1429-1437.
[25] R. Krishna, J.M. van Baten, MD Simulations of Diffusivities in Methanol-n-hexane Mixtures Near the Liquid-liquid Phase Splitting Region, Chem. Eng. Techol. 29(4) (2006) 516-519.
[26] A. Barnard, C.M. Li, R. Zhou, Y. Zhao, Modelling of the nanoscale, Nanoscale 4(4) (2012) 1042-1043.
[27] N.F.A. van der Vegt, W.J. Briels, M. Wessling, H. Strathmann, A nonequilibrium simulation method for calculating tracer diffusion coefficients of small solutes in n-alkane liquids and polymers, J. Chem. Phys. 108(22) (1998) 9558-9565.
[28] M. Heuchel, M. Böhning, O. Hölck, M.R. Siegert, D. Hofmann, Atomistic packing models for experimentally investigated swelling states induced by CO2 in glassy polysulfone and poly(ether sulfone), J. Polym. Sci. Pt. B Polym. Phys. 44(13) (2006) 1874-1897.
[29] O. Hölck, M.R. Siegert, M. Heuchel, M. Böhning, CO2 Sorption Induced Dilation in Polysulfone: Comparative Analysis of Experimental and Molecular Modeling Results, Macromol. 39(26) (2006) 9590-9604.
[30] O. Hölck, M. Heuchel, M. Böhning, D. Hofmann, Simulation of experimentally observed dilation phenomena during integral gas sorption in glassy polymers, J. Polym. Sci. Pt. B Polym. Phys. 46(1) (2008) 59-71.
[31] T. Spyriouni, G.C. Boulougouris, D.N. Theodorou, Prediction of Sorption of CO2 in Glassy Atactic Polystyrene at Elevated Pressures Through a New Computational Scheme, Macromol. 42(5) (2009) 1759-1769.
[32] S. Velioğlu, M.G. Ahunbay, S.B. Tantekin-Ersolmaz, Investigation of CO 2-induced plasticization in fluorinated polyimide membranes via molecular simulation, J. Membr. Sci. 417 (2012) 217-227.
[33] S. Neyertz, D. Brown, The effect of structural isomerism on carbon dioxide sorption and plasticization at the interface of a glassy polymer membrane, J. Membr. Sci. 460 (2014) 213-228.
[34] S. Neyertz, D. Brown, Nanosecond-time-scale reversibility of dilation induced by carbon dioxide sorption in glassy polymer membranes, J. Membr. Sci. 520 (2016) 385-399.
[35] M. Safari, A. Ghanizadeh, M.M. Montazer-Rahmati, Optimization of membrane-based CO2-removal from natural gas using simple models considering both pressure and temperature effects, Int. J. Greenh. Gas Cont. 3(1) (2009) 3-10.
[36] Y. Huang, D.R. Paul, Effect of Temperature on Physical Aging of Thin Glassy Polymer Films, Macromol. 38(24) (2005) 10148-10154.
[37] S.S.M. Lock, K.K. Lau, A.M. Shariff, Y.F. Yeong, Joule Thomson Effect in a Two-dimensional Multi-component Radial Crossflow Hollow Fiber Membrane Applied for CO2 Capture in Natural Gas Sweetening, Process Systems and Materials for CO2 Capture, John Wiley & Sons, Ltd2017, pp. 371-397.
[38] X. Duthie, S. Kentish, C. Powell, K. Nagai, G. Qiao, G. Stevens, Operating temperature effects on the plasticization of polyimide gas separation membranes, J. Membr. Sci. 294(1–2) (2007) 40-49.
[39] N.R. Horn, D.R. Paul, Carbon Dioxide Sorption and Plasticization of Thin Glassy Polymer Films Tracked by Optical Methods, Macromol. 45(6) (2012) 2820-2834.
[40] N.R. Horn, D.R. Paul, Carbon dioxide plasticization of thin glassy polymer films, Polym. 52(24) (2011) 5587-5594.
[41] A. Jamil, O.P. Ching, A.M. Shariff, Current Status and Future Prospect of Polymer-Layered Silicate Mixed-Matrix Membranes for CO2/CH4 Separation, Chem. Eng. Techol. 39(8) (2016) 1393-1405.

[42] A. Fernández-Barquín, C. Casado-Coterillo, M. Etxeberria-Benavides, J. Zuñiga, A. Irabien, Comparison of Flat and Hollow-Fiber Mixed-Matrix Composite Membranes for CO2 Separation with Temperature, Chem. Eng. Techol. 40(5) (2017) 997-1007.
[43] S.S.M. Lock, K.K. Lau, A.M. Shariff, Y.F. Yeong, Preliminary techno-economic and environmental assessment of thickness dependent physical aging in oxygen enriched combustion using polymeric membranes, J. Clean. Prod.
[44] H.A. Mannan, H. Mukhtar, T. Murugesan, R. Nasir, D.F. Mohshim, A. Mushtaq, Recent Applications of Polymer Blends in Gas Separation Membranes, Chem. Eng. Techol. 36(11) (2013) 1838-1846.
[45] S.S.M. Lock, K.K. Lau, A.M. Shariff, Mathematical Modeling of the Radial Crossflow Hollow Fiber Membrane Module for Multi-Component Gas Separation, Appl. Mech. Mater. 625 (2014) 726-729.
[46] S.S.M. Lock, K.K. Lau, A.M. Shariff, Effect of recycle ratio on the cost of natural gas processing in countercurrent hollow fiber membrane system, J. Ind. Eng. Chem. 21 (2015) 542-551.
[47] P.J. in 't Veld, M.T. Stone, T.M. Truskett, I.C. Sanchez, Liquid Structure via Cavity Size Distributions, J. Phys. Chem. B 104(50) (2000) 12028-12034.
[48] H.F. Ridgway, J.D. Gale, Z.E. Hughes, M.B. Stewart, J.D. Orbell, S.R. Gray, Molecular Scale Modelling of Membrane Water Treatment Processes, in: D. Mike, D. Zhao, R. Semiat (Eds.), Functional Nanostructured Materials and Membranes for Water Treatment, Wiley- WCH, Weinheim, Germany, 2013.
[49] K. Golzar, S. Amjad-Iranagh, M. Amani, H. Modarress, Molecular simulation study of penetrant gas transport properties into the pure and nanosized silica particles filled polysulfone membranes, J. Membr. Sci. 451 (2014) 117-134.
[50] S. Ban, C. Huang, X.-Z. Yuan, H. Wang, Molecular Simulation of Gas Adsorption, Diffusion, and Permeation in Hydrated Nafion Membranes, J. Phys. Chem. B 115(39) (2011) 11352-11358.
[51] S.N. Wijenayake, N.P. Panapitiya, S.H. Versteeg, C.N. Nguyen, S. Goel, K.J. Balkus, I.H. Musselman, J.P. Ferraris, Surface Cross-Linking of ZIF-8/Polyimide Mixed Matrix Membranes (MMMs) for Gas Separation, Ind. Eng. Chem. Res. 52(21) (2013) 6991-7001.
[52] N. Jusoh, Y.F. Yeong, K.K. Lau, A. M. Shariff, Enhanced gas separation performance using mixed matrix membranes containing zeolite T and 6FDA-durene polyimide, J. Membr. Sci. 525 (2017) 175-186.
[53] R. Nasir, H. Mukhtar, Z. Man, D.F. Mohshim, Material Advancements in Fabrication of Mixed-Matrix Membranes, Chem. Eng. Techol. 36(5) (2013) 717-727.
[54] S.A. Stern, A.H. De Meringo, Solubility of carbon dioxide in cellulose acetate at elevated pressures, J. Polym. Sci. Pt. B Polym. Phys. 16(4) (1978) 735-751.
[55] Accelrys Software Inc., 2015.
[56] J. Ahn, W.-J. Chung, I. Pinnau, M.D. Guiver, Polysulfone/silica nanoparticle mixed-matrix membranes for gas separation, J. Membr. Sci. 314(1–2) (2008) 123-133.
[57] S.S.M. Lock, K.K. Lau, A.M. Shariff, Y.F. Yeong, A.M. Bustam, Computational insights on the role of film thickness on the physical propertes of ultrathin polysulfone membranes, RSC Adv. 7(70) (2017) 44376-44393.
[58] K. Golzar, S. Amjad-Iranagh, M. Amani, H. Modarress, Molecular simulation study of penetrant gas transport properties into the pure and nano sized silica particles filled polysulfone membranes, J. Membr. Sci. 451 (2014) 117–134.
[59] R. Krishna, J.M. van Baten, Loading Dependence of Self-Diffusivities of Gases in Zeolites, Chem. Eng. Techol. 30(9) (2007) 1235-1241.
[60] W. Cai, J. Li, S. Yip, Molecular Dynamics, in: R.J.M. Konings (Ed.), Comprehensive Nuclear Materials, Elsevier, Amsterdam, 2012, pp. 249-265.
[61] U. Philippe, T. Bernard, B. Anne, Basics for Molecular Simulation, Applications of Molecular Simulation in the Oil and Gas Industry: Monte Carlo Methods, Editions Technip, Paris, 2005, pp. 7-83.
[62] A.N. Gulluoglu, D.J. Srolovitz, R. LeSar, P.S. Lomdahl, Dislocation Distributions in Two Dimensions, Scripta Metall. 23 (1989) 1347-1352.

[63] A. Arnold, C. Holm, Efficient Methods to Compute Long Range Interactions for Soft Matter System, in: C. Holm, K. Kremer (Eds.), Advanced Computer Simulation Approaches for Soft Matter Sciences II, Springer-Verlag, Berlin, 2005, pp. 59-110.
[64] C. Forrey, D.M. Saylor, J.S. Silverstein, J.F. Douglas, E.M. Davis, Y.A. Elabd, Prediction and validation of diffusion coefficients in a model drug delivery system using microsecond atomistic molecular dynamics simulation and vapour sorption analysis, Soft Matter 10(38) (2014) 7480-7494.
[65] J. Kruse, J. Kanzow, K. Rätzke, F. Faupel, M. Heuchel, J. Frahn, D. Hofmann, Free Volume in Polyimides: Positron Annihilation Experiments and Molecular Modeling, Macromol. 38(23) (2005) 9638-9643.
[66] J.R. Fried, Molecular Simulation of Gas and Vapor Transport in Highly Permeable Polymers, in: B. Freeman, Y. Yampolskii, I. Pinnau (Eds.), Materials Science of Membranes for Gas and Vapor Separation, John Wiley & Sons, Chichester 2006, pp. 95-127.
[67] S. Yang, J. Choi, M. Cho, Elastic Stiffness and Filler Size Effect of Covalently Grafted Nanosilica Polyimide Composites: Molecular Dynamics Study, ACS Appl. Mat. Int. 4(9) (2012) 4792-4799.
[68] A. Bahramian, Molecular dynamics simulation of surface morphology and thermodynamic properties of polyaniline nanostructured film, Surf. Interface Anal. 47(1) (2015) 1-14.
[69] E. Tocci, P. Pullumbi, Molecular simulation of realistic membrane models of alkylated PEEK membranes, Mol. Sim. 32(2) (2006) 145-154.
[70] M. Heuchel, D. Hofmann, Molecular modelling of polyimide membranes for gas separation, Desalination 144(1) (2002) 67-72.
[71] Y. Mo, H. Zhang, J. Xu, Molecular dynamic simulation of the mechanical properties of PI/SiO2 nanocomposite based on materials studio J. Chem. Pharm. Res. 6(6) (2014) 1534-1539.
[72] M. Farhadinia, B. Arab, J.E. Jam, Mechanical Properties of CNT-Reinforced Polymer Nanocomposites: A Molecular Dynamics Study, Mech. Adv. Composite Struc. 3(2) (2016) 113-121.
[73] S.S.M. Lock, K.K. Lau, A.M. Shariff, Y.F. Yeong, M.A. Bustam, Thickness dependent penetrant gas transport properties and separation performance within ultrathin polysulfone membrane: Insights from atomistic molecular simulation, j. Polym. Sci. Pt. B Polym. Phys.
[74] P. Zoller, Specific volume of polysulfone as a function of temperature and pressure, J. Polym. Sci. Polym. Phys. Ed. 16(7) (1978) 1261-1275.
[75] R.F. Cracknell, D. Nicholson, Grand canonical Monte Carlo study of Lennard-Jones mixtures in slit pores. Part 3.-Mixtures of two molecular fluids: ethane and propane, J. Chem. Soc. Faraday Trans. 90(11) (1994) 1487-1493.
[76] H. Hu, X. Li, Z. Fang, N. Wei, Q. Li, Small-molecule gas sorption and diffusion in coal: Molecular simulation, Energ. 35(7) (2010) 2939-2944.
[77] M. Rahmati, H. Modarress, R. Gooya, Molecular simulation study of polyurethane membranes, Polym. 53(9) (2012) 1939-1950.
[78] Q.L. Liu, Y. Huang, Transport Behavior of Oxygen and Nitrogen through Organasilicon-Containing Polystyrenes by Molecular Simulation, J. Phys. Chem. B 110(35) (2006) 17375-17382.
[79] N. Metropolis, A.W. Rosenbluth, M.N. Rosenbluth, A.H. Teller, E. Teller, Equation of State Calculations by Fast Computing Machines, J. Chem. Phys. 21(6) (1953) 1087-1092.
[80] J.I. Siepmann, D. Frenkel, Configurational bias Monte Carlo: a new sampling scheme for flexible chains, Mol. Phys. 75(1) (1992) 59-70.
[81] P.M. Budd, N.B. Mckeown, D. Fritsch, Free volume and intrinsic microporosity in polymers, J. Mater. Chem. 15(20) (2005) 1977-1986.
[82] M.A.A.R. Quddus, O.J. Rojas, M.A. Pasquinelli, Molecular Dynamics Simulations of the Adhesion of a Thin Annealed Film of Oleic Acid onto Crystalline Cellulose, Biomacromolecules 15(4) (2014) 1476-1483.
[83] G. Shen, Q. Mei, V.B. Prakapenka, P. Lazor, S. Sinogeikin, Y. Meng, C. Park, Effect of helium on structure and compression behavior of SiO(2) glass, Proc. Natl. Acad. Sci. U.S.A. 108(15) (2011) 6004-6007.

[84] A. Bondi, Physical properties of molecular crystals, liquids and glasses, John Wiley & Sons, New York [etc.], 1968.
[85] D.W. Van Krevelen, CHAPTER 4 - VOLUMETRIC PROPERTIES, Properties of Polymers (Third, completely revised edition), Elsevier, Amsterdam, 1997, pp. 71-107.
[86] E. Sada, H. Kumazawa, P. Xu, M. Nishigaki, Mechanism of gas permeation through glassy polymer films, J. Membr. Sci. 37(2) (1988) 165-179.
[87] W.J. Koros, D.R. Paul, CO2 sorption in poly(ethylene terephthalate) above and below the glass transition, J. Polym. Sci. Part B Polym. Phys. 16(11) (1978) 1947-1963.
[88] L.M. Costello, W.J. Koros, Temperature dependence of gas sorption and transport properties in polymers: measurement and applications, Ind. Eng. Chem. Res. 31(12) (1992) 2708-2714.
[89] A.E. Gemeda, M.G. De Angelis, N. Du, N. Li, M.D. Guiver, G.C. Sarti, Mixed gas sorption in glassy polymeric membranes. III. CO2/CH4 mixtures in a polymer of intrinsic microporosity (PIM-1): Effect of temperature, J. Membr. Sci. 524 (2017) 746-757.
[90] K.A. Stevens, Z.P. Smith, K.L. Gleason, M. Galizia, D.R. Paul, B.D. Freeman, Influence of temperature on gas solubility in thermally rearranged (TR) polymers, J. Membr. Sci. 533 (2017) 75-83.
[91] R.M. Barrer, J.A. Barrie, J. Slater, Sorption and diffusion in ethyl cellulose. Part III. Comparison between ethyl cellulose and rubber, J. Polym. Sci. 27(115) (1958) 177-197.
[92] W.J. Koros, D.R. Paul, A.A. Rocha, Carbon dioxide sorption and transport in polycarbonate, J. Polym. Sci. 14(4) (1976) 687-702.
[93] B.J. Story, W.J. Koros, Comparison of three models for permeation of CO2/CH4 mixtures in poly(phenylene oxide), J. Polym. Sci. 27(9) (1989) 1927-1948.
[94] H. Lin, B.D. Freeman, Gas solubility, diffusivity and permeability in poly(ethylene oxide), Journal of Membrane Science 239(1) (2004) 105-117.
[95] P.G. Tait, Report on some of the physical properties of fresh water and sea, Report on the scientific results of the voyage of the H.M.S. Challenger during the years 1873-76, Phys. Chem. 2 (1988) 1-76.
[96] P. Zoller, A study of the pressure-volume-temperature relationships of four related amorphous polymers: Polycarbonate, polyarylate, phenoxy, and polysulfone, J. Polym. Sci. Part B Polym. Phys. 20(8) (1982) 1453-1464.
[97] P. Zoller, Specific volume of polysulfone as a function of temperature and pressure, J. Polym. Sci. Part B Polym. Phys. 16(7) (1978) 1261-1275.
[98] A. Bos, I.G.M. Pünt, M. Wessling, H. Strathmann, CO2-induced plasticization phenomena in glassy polymers, J. Membr. Sci. 155(1) (1999) 67-78.
[99] C. Li, G.A. Medvedev, E.-W. Lee, J. Kim, J.M. Caruthers, A. Strachan, Molecular dynamics simulations and experimental studies of the thermomechanical response of an epoxy thermoset polymer, Polym. 53(19) (2012) 4222-4230.
[100] A. Ebadi Amooghin, P. Moradi Shehni, A. Ghadimi, M. Sadrzadeh, T. Mohammadi, Mathematical modeling of mass transfer in multicomponent gas mixture across the synthesized composite polymeric membrane, J. Ind. Eng. Chem. 19(3) (2013) 870-885.
[101] W.J. Koros, D.R. Paul, G.S. Huvard, Energetics of gas sorption in glassy polymers, Polym. 20(8) (1979) 956-960.
[102] C.A. Scholes, G.Q. Chen, G.W. Stevens, S.E. Kentish, Plasticization of ultra-thin polysulfone membranes by carbon dioxide, J. Membr. Sci. 346(1) (2010) 208-214.
[103] Y. Huang, D.R. Paul, Physical aging of thin glassy polymer films monitored by gas permeability, Polym. 45(25) (2004) 8377-8393.
[104] Y. Huang, D.R. Paul, Physical Aging of Thin Glassy Polymer Films Monitored by Optical Properties, Macromol. 39(4) (2006) 1554-1559.
[105] Y. Huang, D.R. Paul, Effect of Film Thickness on the Gas-Permeation Characteristics of Glassy Polymer Membranes, Ind. Eng. Chem. Res. 46(8) (2007) 2342-2347.

[106] W.-C.V. Wang, E.J. Kramer, W.H. Sachse, Effects of high-pressure CO2 on the glass transition temperature and mechanical properties of polystyrene, J. Polym. Sci. Pt. B Polym. Phys. 20(8) (1982) 1371-1384.
[107] J.S. Chiou, J.W. Barlow, D.R. Paul, Plasticization of glassy polymers by CO2, J. Appl. Polym. Sci. 30(6) (1985) 2633-2642.
[108] P. Alessi, A. Cortesi, I. Kikic, F. Vecchione, Plasticization of polymers with supercritical carbon dioxide: Experimental determination of glass-transition temperatures, J. Appl. Polym. Sci. 88(9) (2003) 2189-2193.
[109] I.A. Ozkan, A.S. Teja, Phase equilibria in systems with specific CO2–polymer interactions, Fluid Phase Equilibr. 228 (2005) 487-491.
[110] M.Z. Hossain, A.S. Teja, Modeling phase equilibria in CO2+polymer systems, J. Supercrit. Fluids 96 (2015) 313-323.
[111] M.Z. Hossain, A.S. Teja, Correlation/prediction of sorption, swelling, and cloud points in CO2 + polymer systems, J. Supercrit. Fluids 122 (2017) 58-62.
[112] J.H. van't Hoff, E. Cohen, T. Ewan, Studies in chemical dynamics, The Chemical publishing company, California, 1896.
[113] S. Kilic, S. Michalik, Y. Wang, J.K. Johnson, R.M. Enick, E.J. Beckman, Phase Behavior of Oxygen-Containing Polymers in CO2, Macromol. 40(4) (2007) 1332-1341.
[114] J.H. ter Horst, H.J.M. Kramer, P.J. Jansens, Towards a Crystalline Product Quality Prediction Method by Combining Process Modeling and Molecular Simulations, Chem. Eng. Techol. 29(2) (2006) 175-181.
[115] X. He, D.R. Nieto, A. Lindbråthen, M.-B. Hägg, Membrane System Design for CO2 Capture, Process Systems and Materials for CO2 Capture, John Wiley & Sons, Ltd2017, pp. 249-281.
[116] L. Yan, X.P. Zhang, S.J. Zhang, The Study of Molecular Modeling for Heavy Oil Thermal Cracking, Chem. Eng. Techol. 30(9) (2007) 1166-1175.